The Abdus Salam International Centre for Theoretical Physics

United Nations Educational, Scientific and Cultural Organization

IAEA International Atomic Energy Agency

2272-7

Joint ICTP-IAEA School on Synchrotron Applications in Cultural Heritage and Environmental Sciences and Multidisciplinary Aspects of Imaging Techniques

21 - 25 November 2011

SR based imaging techniques for 3D quantitative analysis of materials

Lucia Mancini

Sincrotrone, Trieste
Italy

Strada Costiera 11, 34151 Trieste, Italy - Tel.+39 040 2240 111; Fax +39 040 224 163 - sci_info@ictp.it

SR based imaging techniques for 3D quantitative analysis of materials

Lucia Mancini

Sincrotrone Trieste, S.S. 14 km 163.5 in AREA Science Park
34049 Basovizza (TS), Italy

lucia.mancini@elettra.trieste.it

http://www.elettra.trieste.it/experiments/beamlines/syrmep/

The Italian synchrotron light laboratory - Elettra

elettra

http://www.elettra.trieste.it

The SYRMEP beamline @ Elettra

Designed and constructed in collaboration with *INFN* and the *Physics Dept. of Università di Trieste.* Devoted to **absorption** and **phase-sensitive** hard **X-ray imaging techniques.**

Medical applications

- *ex-vivo* experiments
- *in-vivo* studies → mammography
  → small animals

Material science and cultural heritage studies

- study of microstructural properties → in a very large range of materials
- *in-situ* and real-time experiments → growth processes
  → mechanical and thermal treatments
  → phase transitions ….

The SYRMEP beamline layout

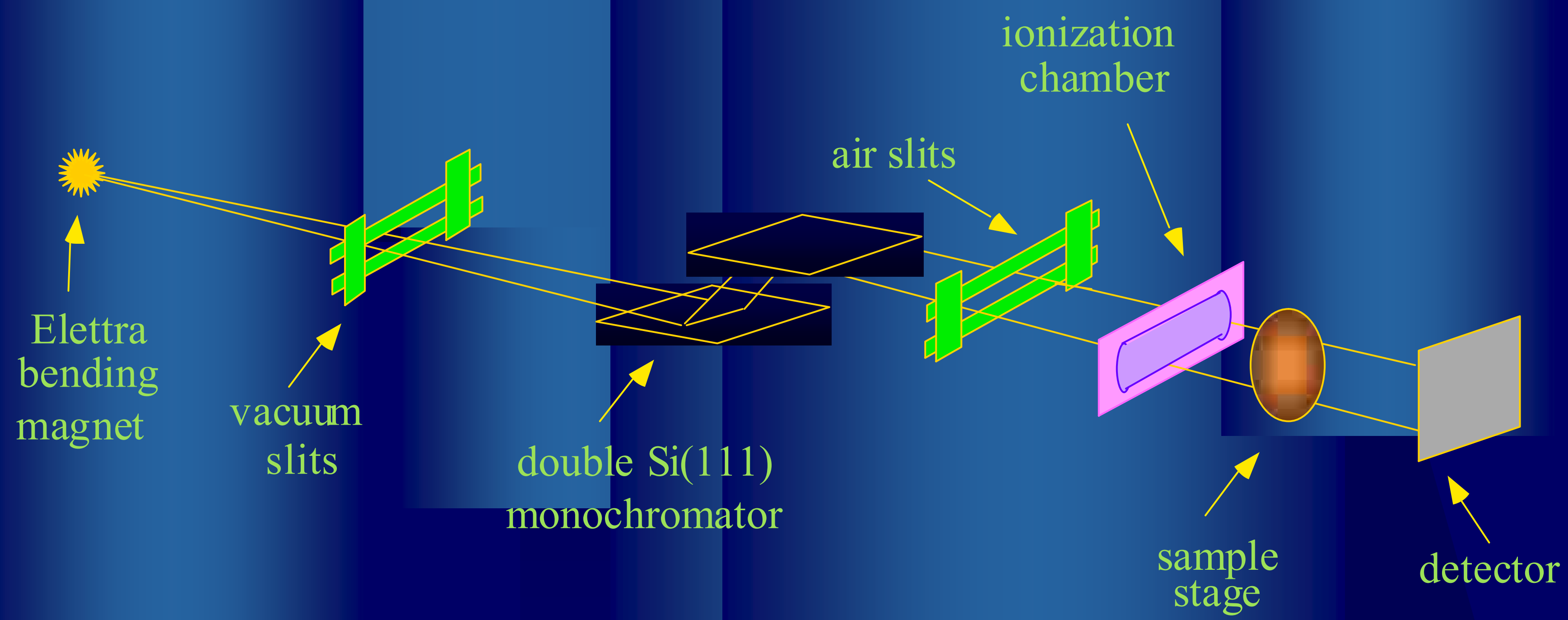

- Energy range: **8.3 ÷ 35 keV**, Bandwidth **$\Delta E/E \cong 2\times10^{-3}$**
- Beam size at sample (h x v) ≅ **150 mm x 4-6 mm**
- Source size (FWHM) s (h x v) ≅ **230 μm x 80 μm**
- Typical fluxes @15 keV ≅ $7 * 10^{8}$ phot./mm^{2} s (@ 2.4 GeV, 180 mA)
- Source-to-sample distance: **D ≅ 23 m**

Why X-ray imaging at a 3rd generation SR facility?

- high energy photons and high flux
  $\rightarrow$ **heavy** and/or **bulky samples** in transmission geometry
  $\rightarrow$ **tunability** in a large energy range (dose reduction)
  $\rightarrow$ **short** exposure times

- small angular source size and big source-to-sample distance
  $\rightarrow$ **high spatial resolution** ($\rho = s\, d / D <\approx 1$ µm at SYRMEP)
  $\rightarrow$ possibility of **big sample-to-detector distances** ($d <\approx 1$m at SYRMEP)
  $\rightarrow$ **high** spatial **coherence** of the X beam ($L_c = \lambda\, D/(2\, s) \cong 10$µm @15keV)

Phase-sensitive techniques

Absorption and Phase-Contrast radiography

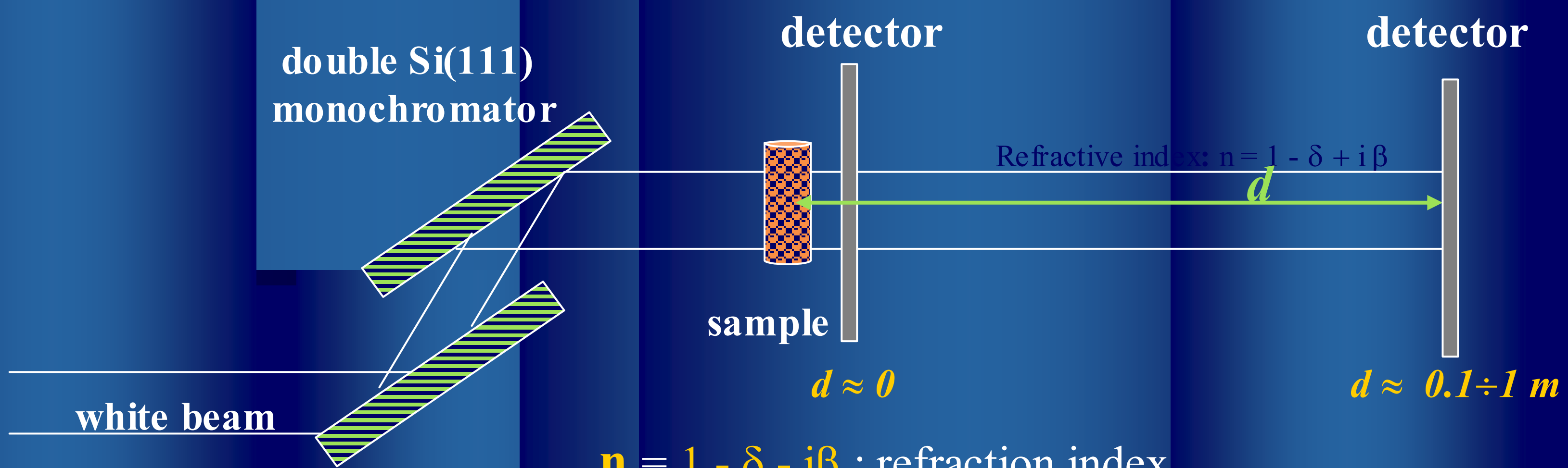

n = 1 - δ - iβ : refraction index

$(\Delta I/I)_{abs} = e^{c\,\Delta\mu} - 1$

$\mu = 4\pi\beta/\lambda$: linear absorption coeff.

c : object size // to beam direction

$\Delta\phi = 2\pi\, c\, \Delta\delta / \lambda$

Fresnel diffraction

$r \ll a \Rightarrow$ *edge detection regime*

$r \cong a \Rightarrow$ *holographic regime*

$r \gg a \Rightarrow$ *Fraunhofer diffraction*

a : object size ⊥ to beam direction

$r = (\lambda d)^{1/2}$: first Fresnel zone radius

Phase vs. amplitude effects with hard X-rays

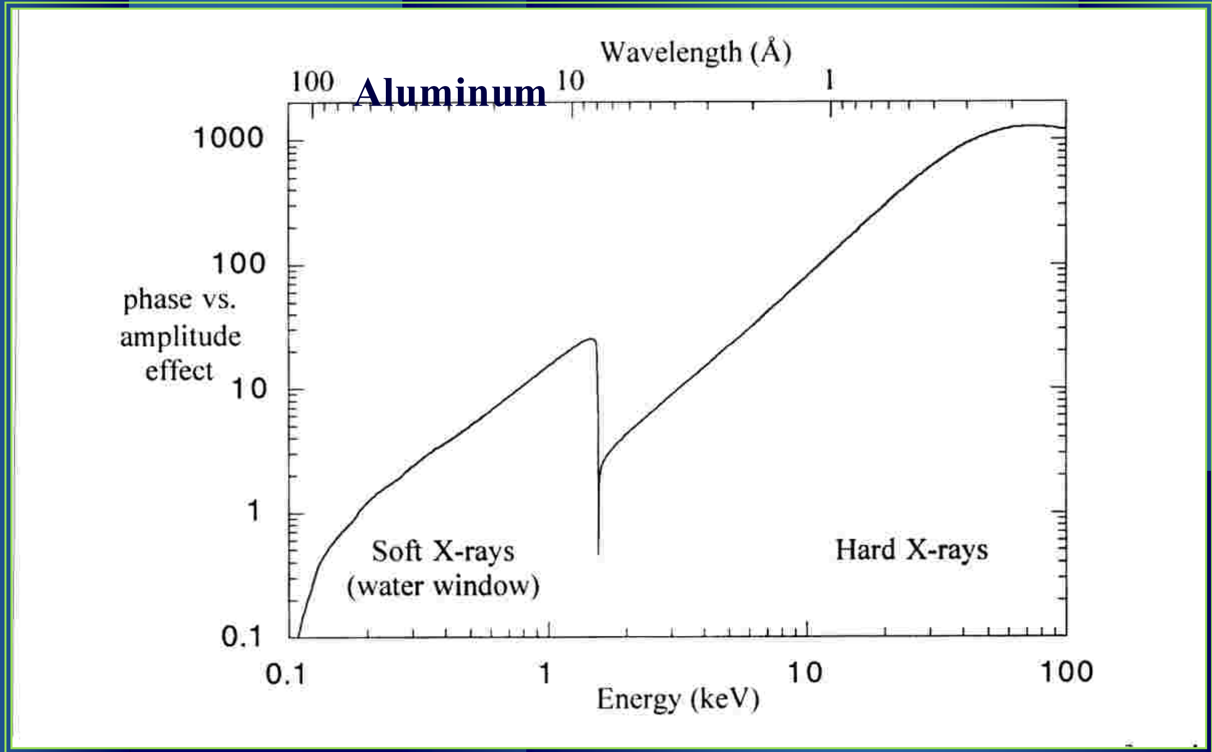

Thus it may be possible to observe phase contrast when absorption contrast is undetectable

Images of a Mimosa flower *(D. Dreossi & co.)*

@ 10 keV

Absorption image

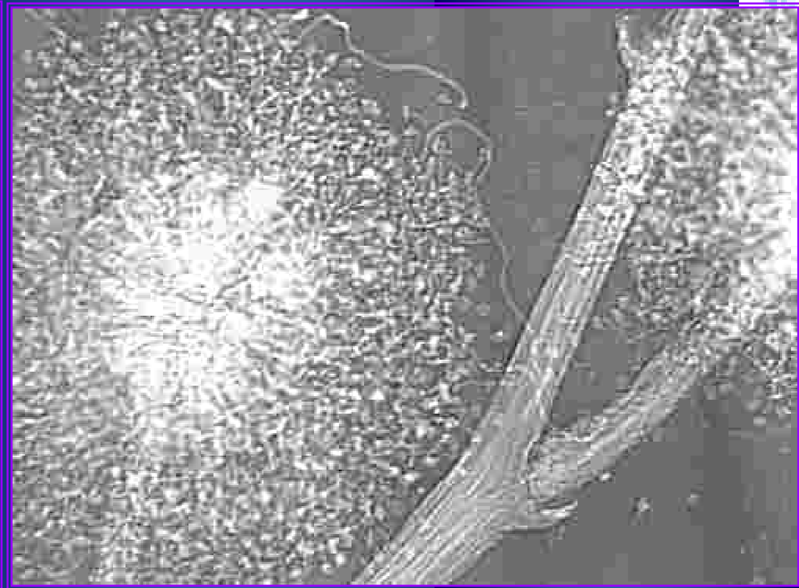

Phase-contrast image

@ 25 keV

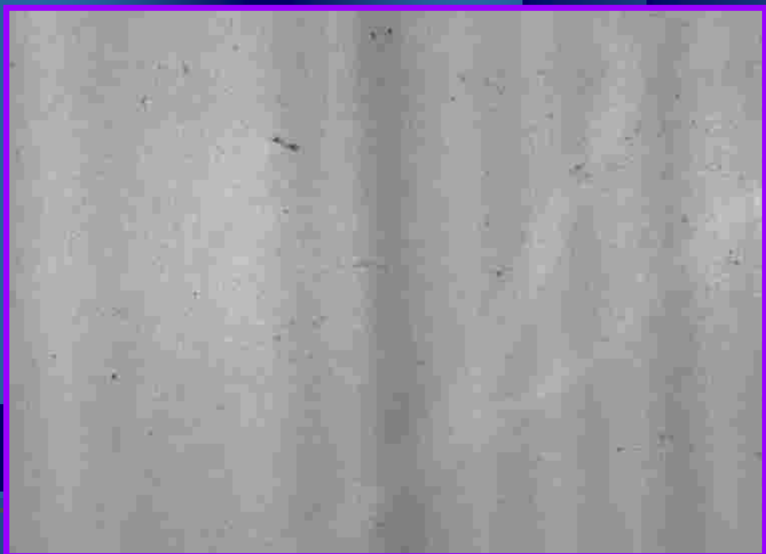

Absorption image

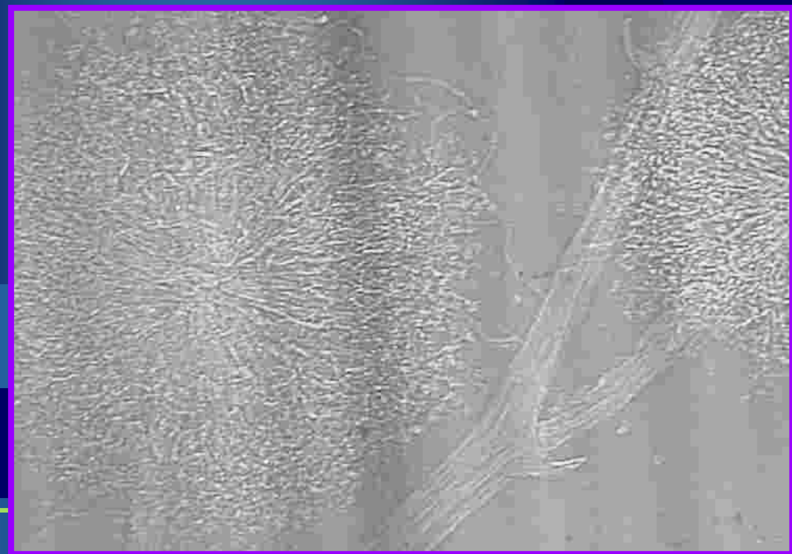

Phase-contrast image

Radiographs of an AlPdMn grain recorded at the ESRF (France)

Mancini L., PhD Thesis, 1998
Mancini L. et al., Phil. Mag. A 78 (1998) 1175

Absorption radiograph

Phase radiograph

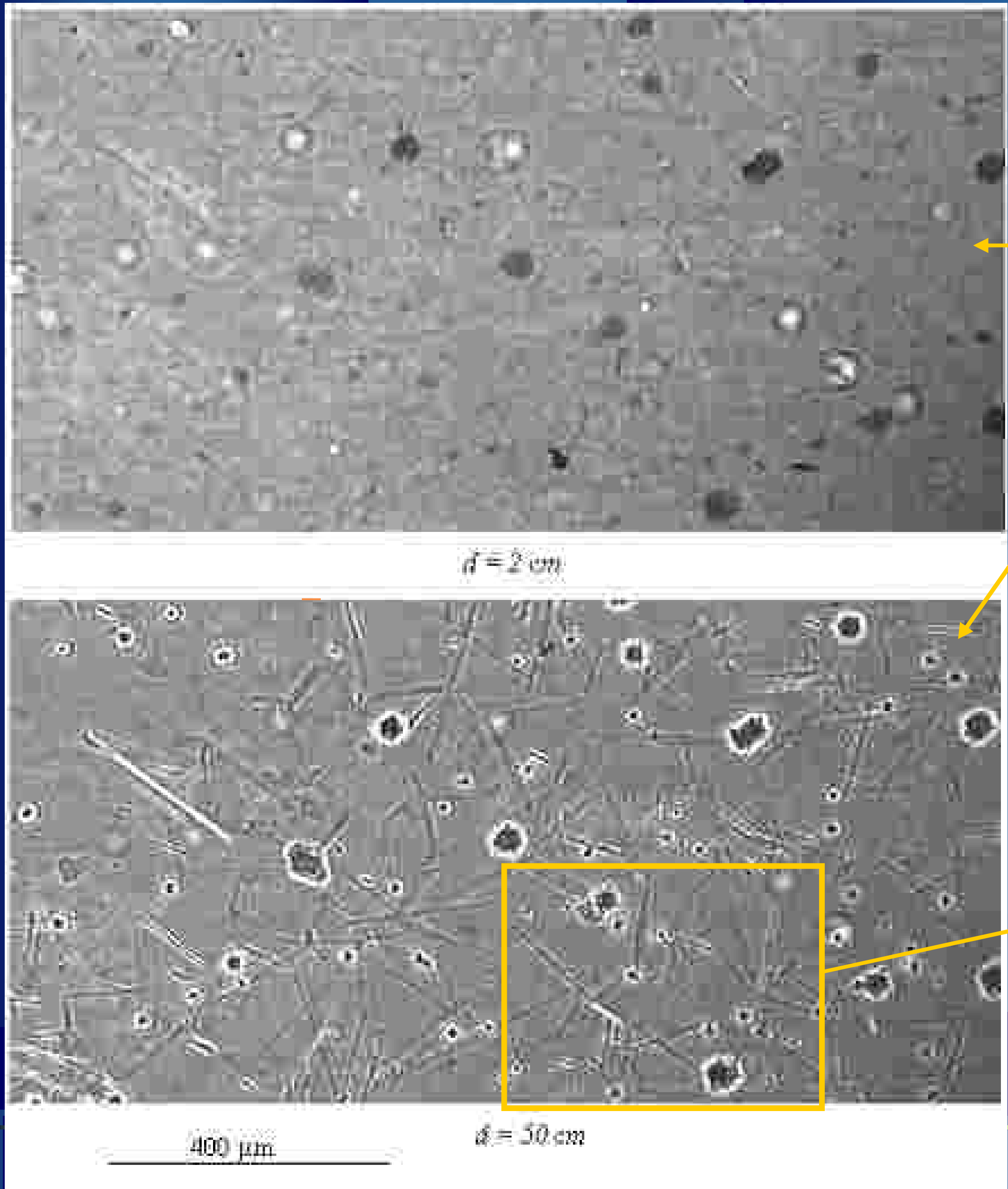

E = 35.5 keV

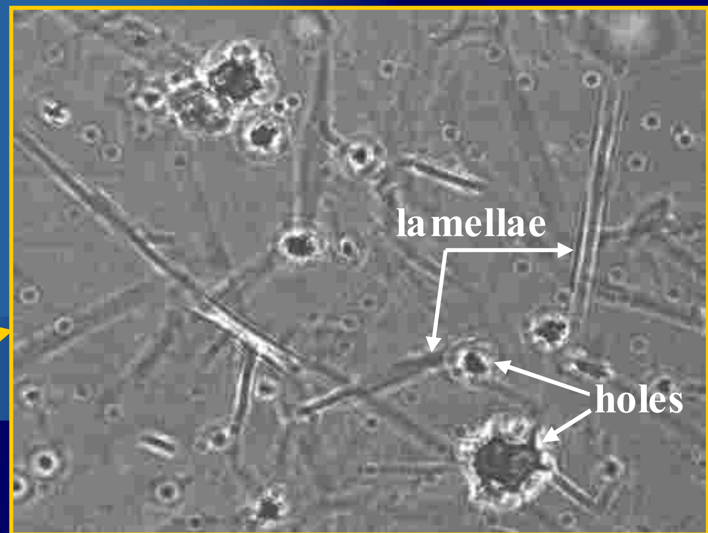

200 µm

The Diffraction Enhanced Imaging (DEI) technique and the PHASY project

PHASY: supported by the EC under Contract No HPRI-1999-CT-50008
coordinator Dr. R.-H. Menk (ELETTRA)

DEI or Analyzer Based Imaging (ABI)

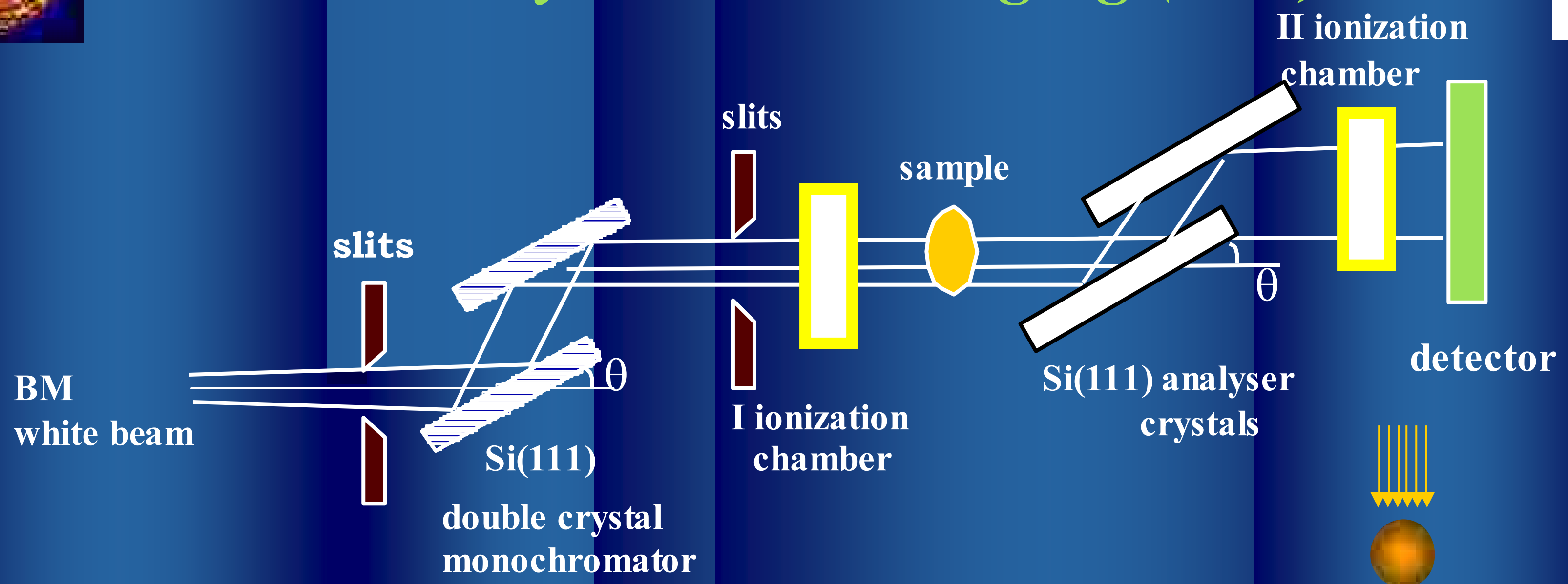

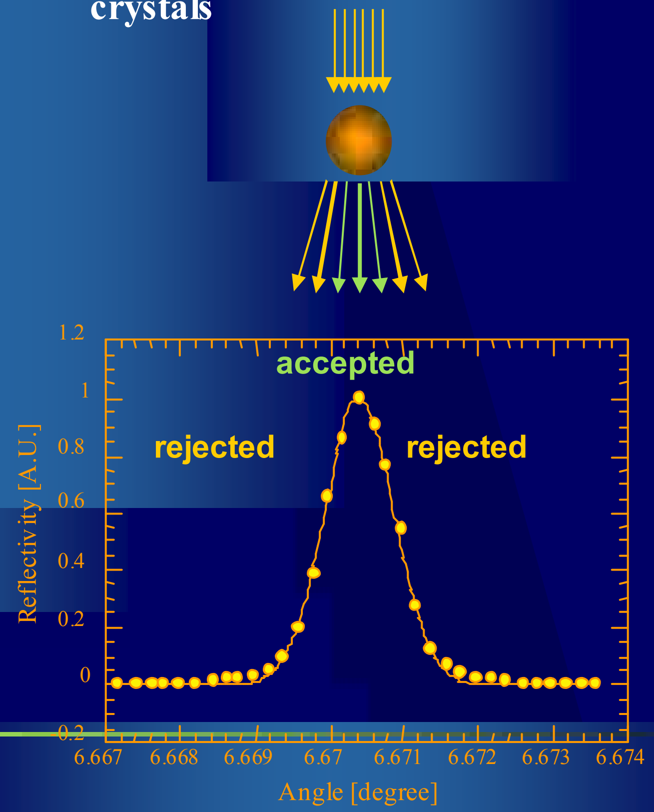

- An **analyzer** between sample and detector used as angular filter to select angular emission of X-rays. The filtering function is the rocking curve (**FWHM: 1-20 μrad**). The detector collects the beam **diffracted** by the analyzer crystal.
- Image formation sensitive to variations of δ in the sample. Refraction angle roughly proportional to the **gradient of** δ.

DEI theory

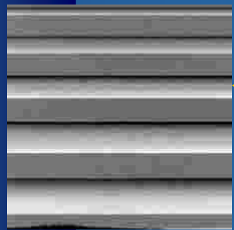

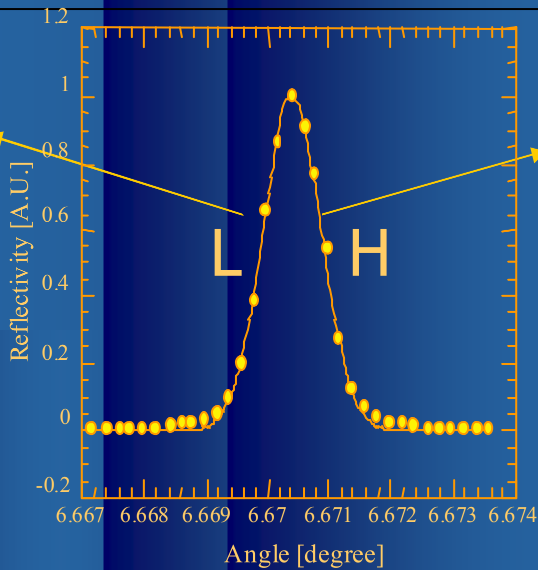

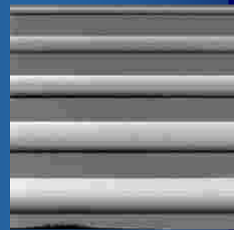

$$I_L = I_R\left(R(\Theta_L) + \frac{\partial R}{\partial \Theta}(\Theta_L)\Delta\Theta_z\right)$$

$$I_H = I_R\left(R(\Theta_H) + \frac{\partial R}{\partial \Theta}(\Theta_H)\Delta\Theta_z\right)$$

I_R = **apparent absorption image**

$\Delta\Theta_Z$ = **refraction image** in the plane of the object

$$I_R = \frac{I_L \cdot \left.\frac{dR}{d\Theta}\right|_{\Theta_H} - I_H \cdot \left.\frac{dR}{d\Theta}\right|_{\Theta_L}}{R(\Theta_L)\cdot\left.\frac{dR}{d\Theta}\right|_{\Theta_H} - R(\Theta_H)\cdot\left.\frac{dR}{d\Theta}\right|_{\Theta_L}}$$

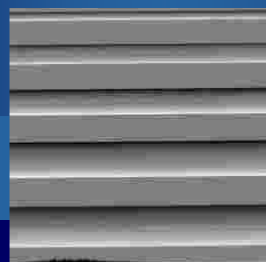

$$\Delta\Theta_Z = \frac{I_H \cdot R(\Theta_L) - I_L \cdot R(\Theta_H)}{I_L \cdot \left.\frac{dR}{d\Theta}\right|_{\Theta_H} - I_H \cdot \left.\frac{dR}{d\Theta}\right|_{\Theta_L}}$$

Human index finger proximal interphalangeal joint

Apparent absorption Image

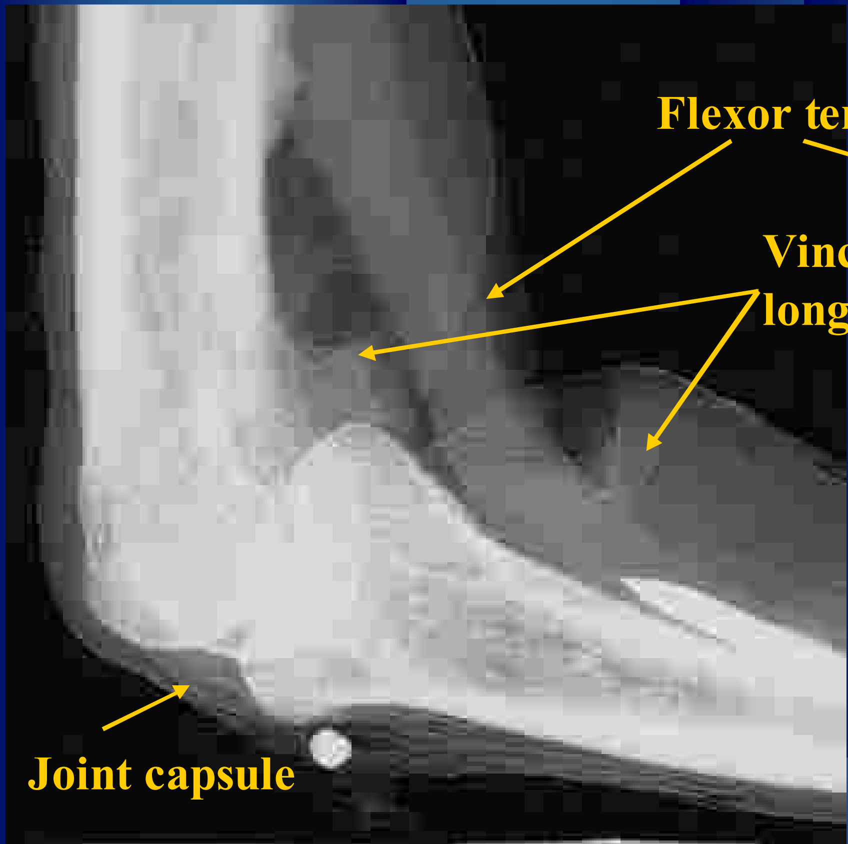

Refraction Image

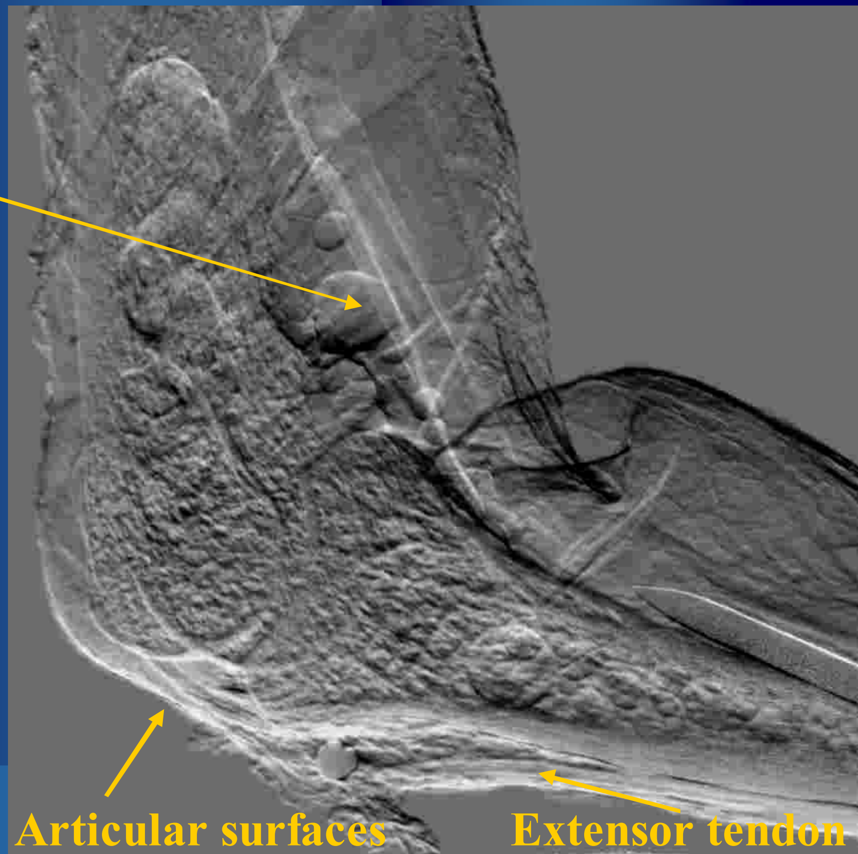

C. J. Hall et al., Elettra highlights (2001) p. 12

Collagen arcades structure in femur head core cuts

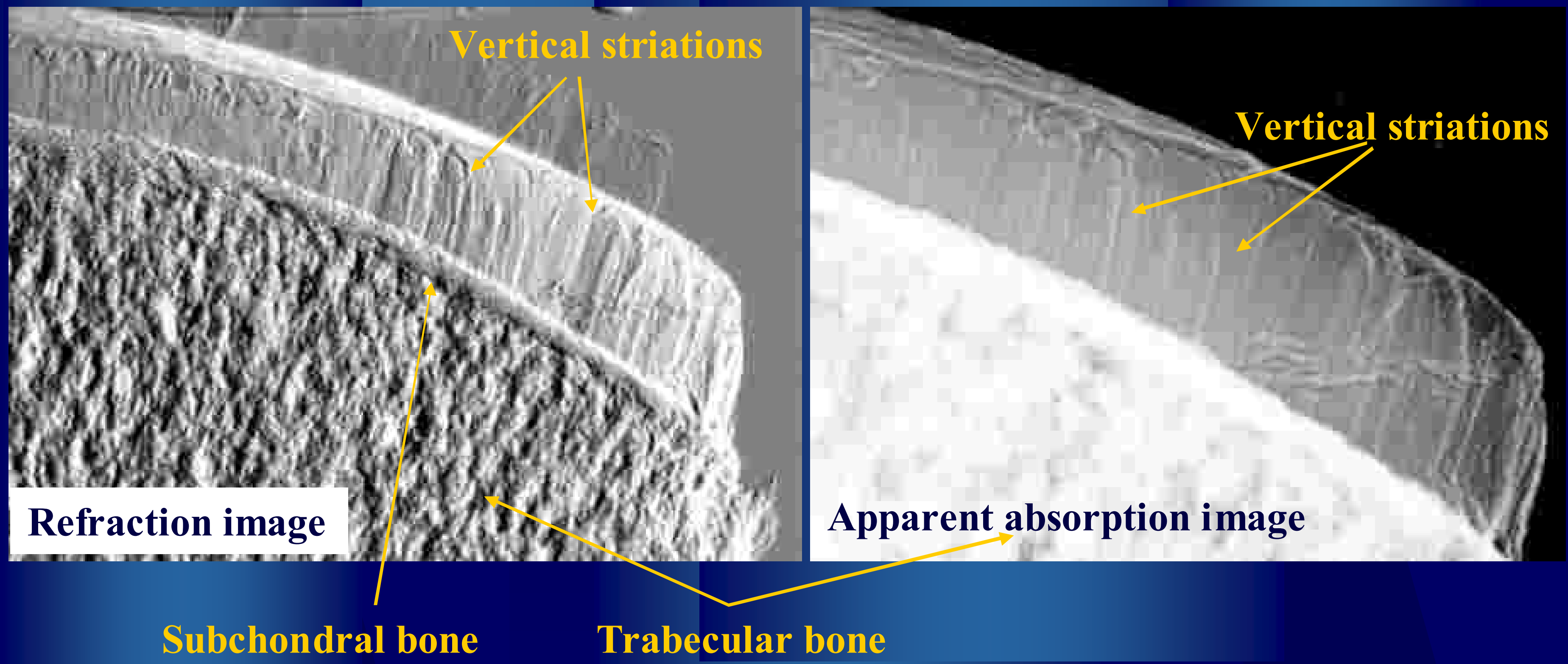

- Collagen fibers switch from horizontal to vertical orientation increasing stiffness and material density

A. Wagnera, et al., Nuclear Instruments and Methods A 548 (2005) 47–53.

Mouse lungs in DEI

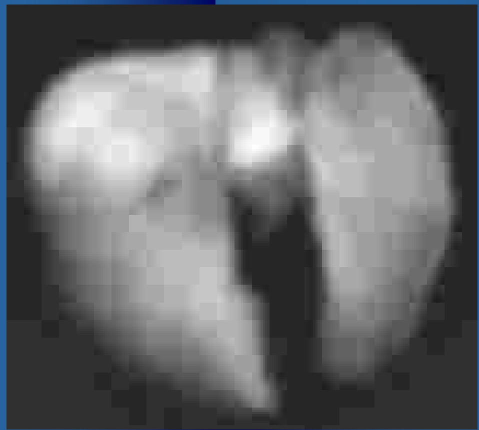

Transmission image

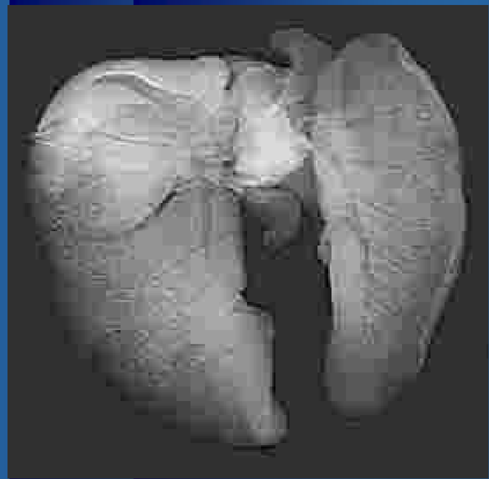

Apparent absorption image

Refraction image

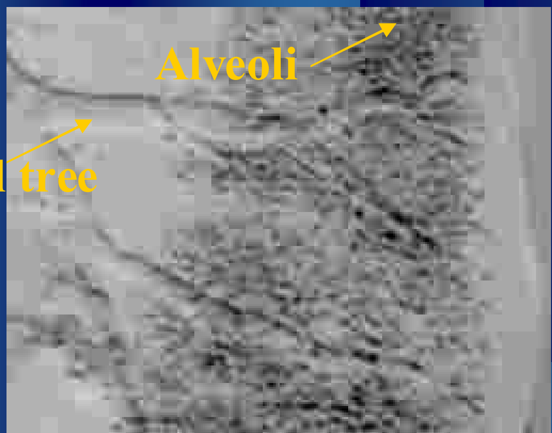

Zoom extinction contrast

Zoom reverse contrast

R.A. Lewis et al., Brit. J. Radiol., 76 (2003) 301–308

Synchrotron X-ray computed microtomography (μ -CT)

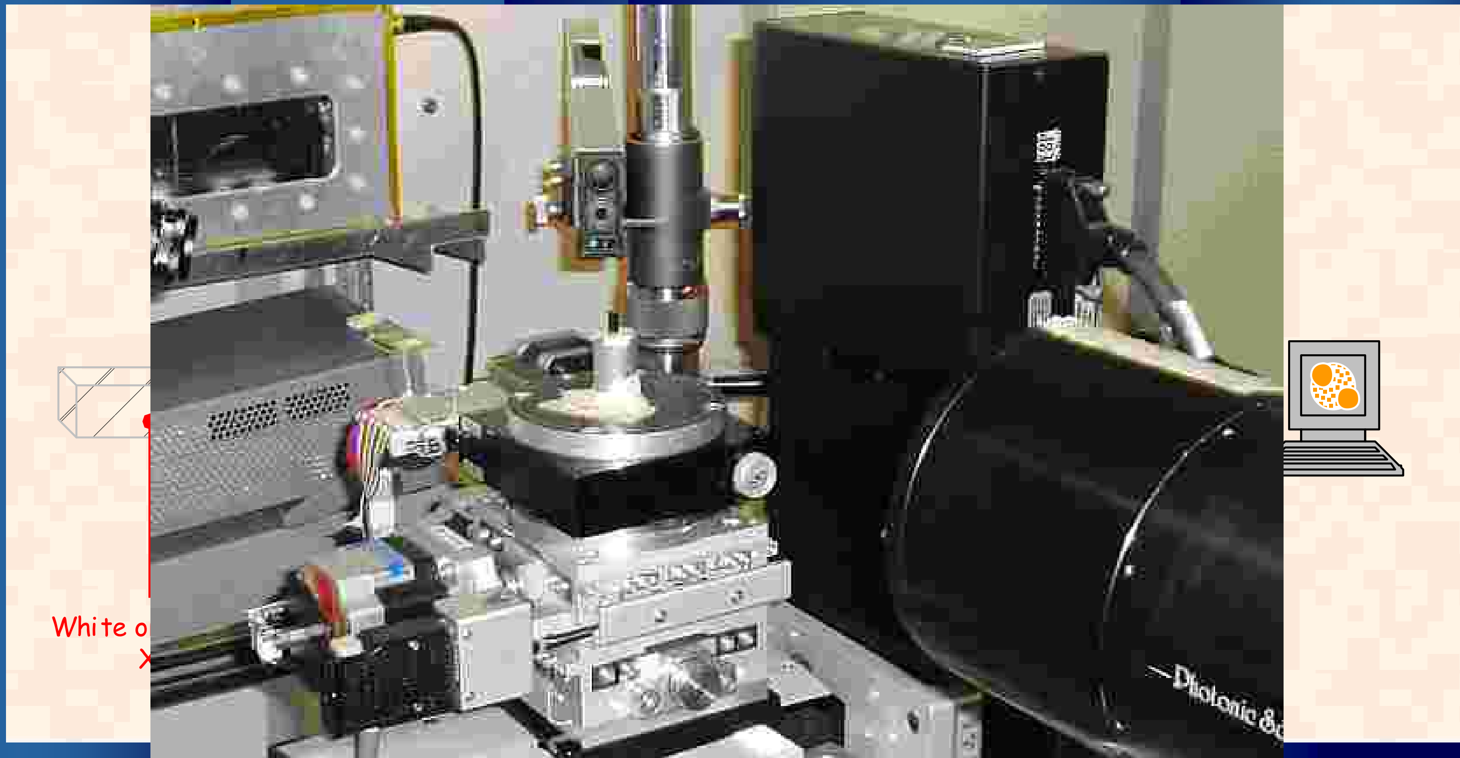

- **Precious** for investigation of **internal features without** sample **sectioning**:
  - → in many cases the **sectioning procedure** modifies the sample structure
  - → the sample can be after **studied by other** experimental **techniques**,
  - → or submitted to several **treatments** (mechanical, thermal, etc...)

CCD detectors & optics

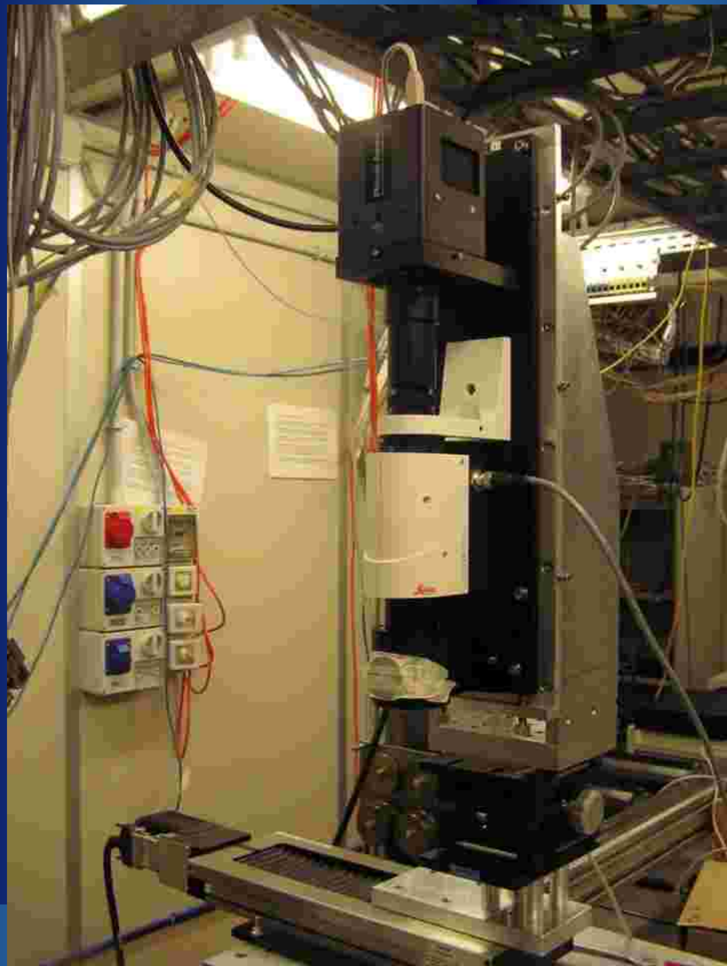

- Photonic Science HYSTAR
  - **16 bit**, **2048** x **2048** pixels^2
  - pixel size: (3.85) 14 x (3.85) 14 µm^2
  - **FOV**: (8) 28 mm x (8) 28 mm
- Photonic Science VHR
  - **12 bit**, **4008** x **2672** pixels^2
  - effective pixel size: 4.5x4.5 µm^2
  - **FOV**: 18 mm x 12 mm
- Photonic Science Lens-coupled
  - **16 bit**, **2048** x **2048** pixels^2
  - pixel size: 7.4x7.4 µm^2
  - **FOV**: continuously adjustable

Optics upgrade: access to white beam for HR imaging

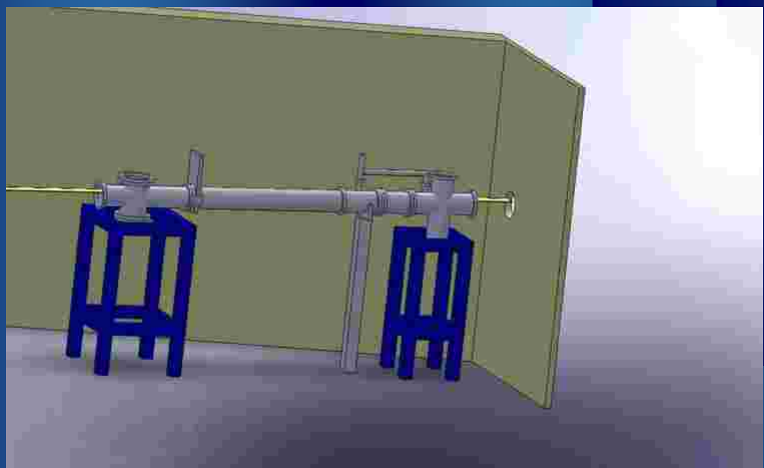

Monochromatic beam mode
(previous set-up)

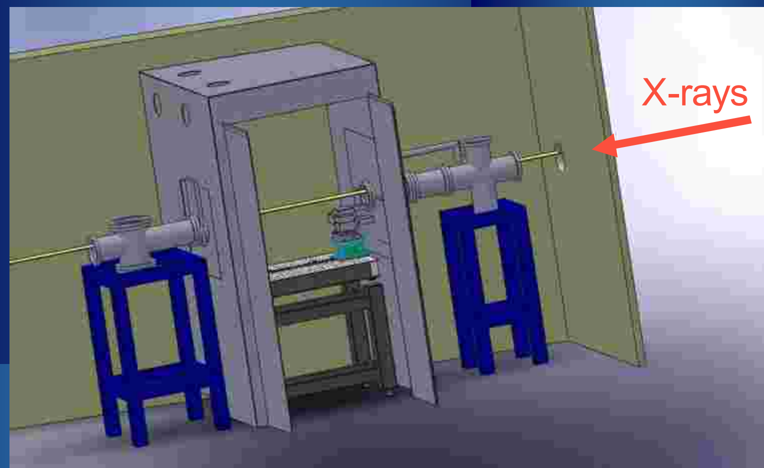

White beam operating mode

TOMOLAB: a conventional μ-CT station at Elettra

Designed at ***Elettra*** and constructed in collaboration with Georesources Dept. and Corso di Laurea in Odontoiatria e Protesi Dentaria - Facoltà Medicina e Chirurgia of the ***Università of Trieste***.

V = **40÷130 kV**, P_{max} = **39 W**, focal $spot_{min}$ = **5 μm**

Elaboration of tomographic images

- Planar radiographs are elaborated by a **reconstruction procedure**:
  → **filtered backprojection** algorithm *[Herman, 1980]*
  → for each projection an **intensity map** is recorded in the xy detector plane
  → projections are submitted to **filtering procedures**
  → each intensity map is **back projected** along the normal to the projection itself
  → finally, the intensities are added for all the projections

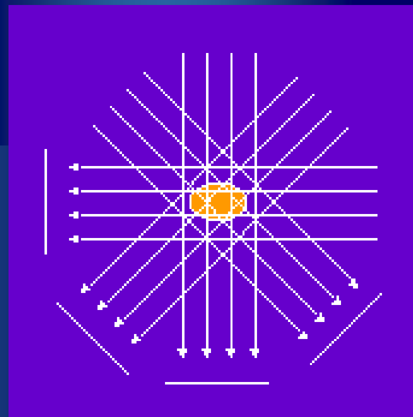

- Reconstructed slices are then treated by a **rendering procedure**:
  → 2D slices visualized as **Stack**
  → 3D views of the sample can be obtained (**Volume rendering**)

- Rendered images can be elaborated applying filters, false colors, **segmentation tools** to extract quantitative information.

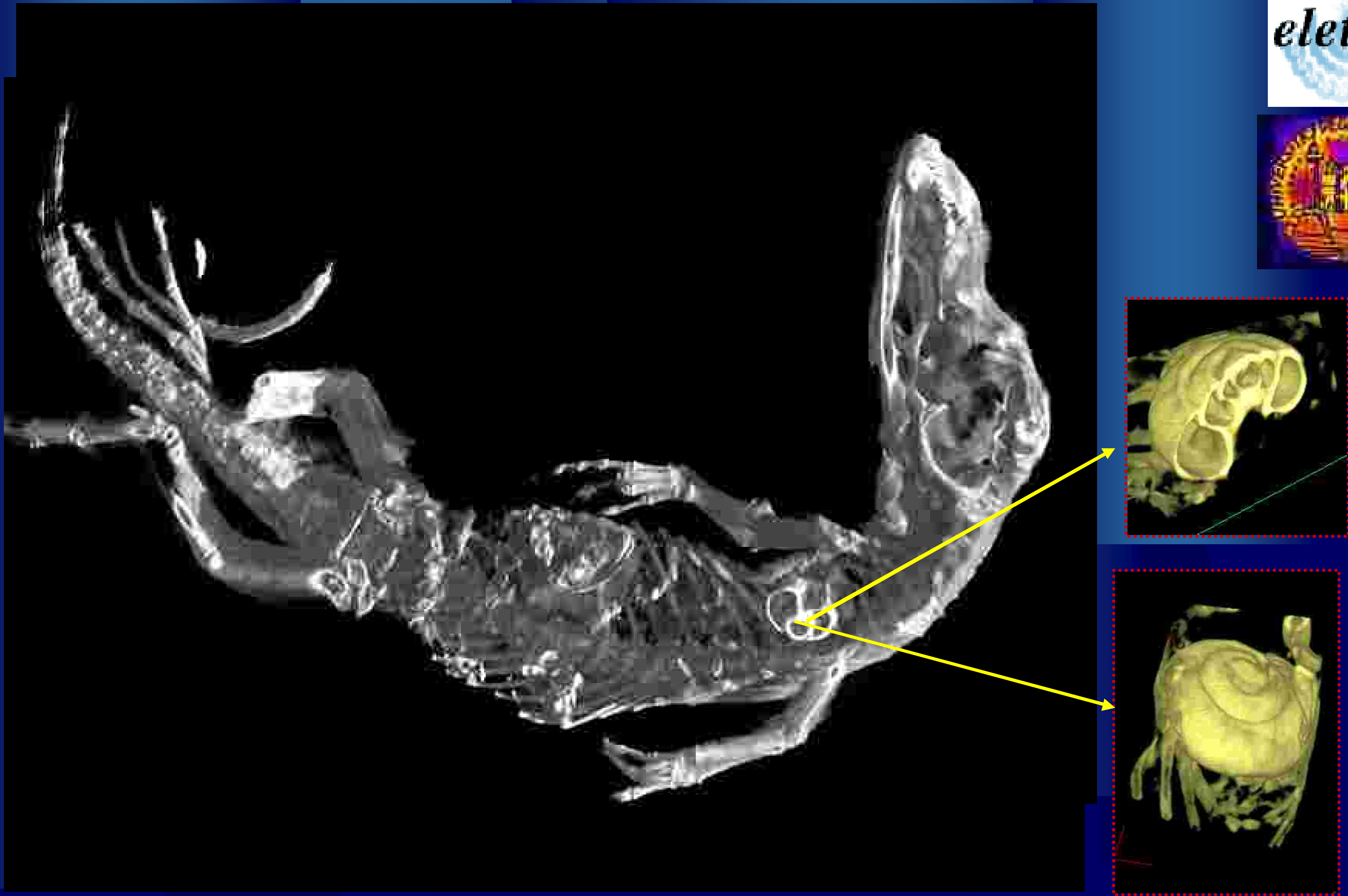

Lucertola

Biomaterials

Implanted bone

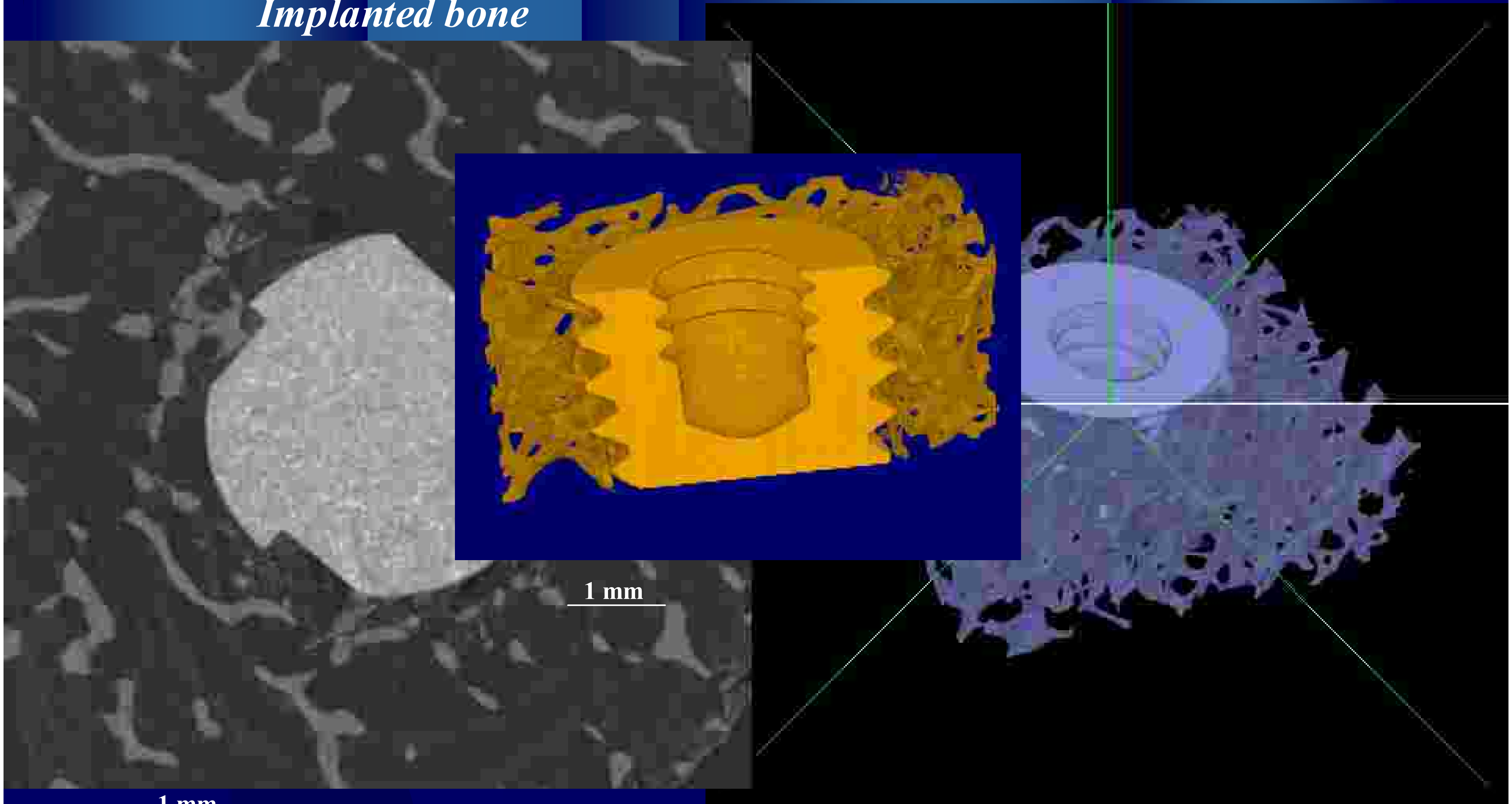

1 mm

E = 29 keV, *d* = 17 cm

L. Tesei et al., Nucl. Instrum. and Meth. A, Vol. 548, Issues 1-2 (2005) 257-263.

Food science

Bread crumb

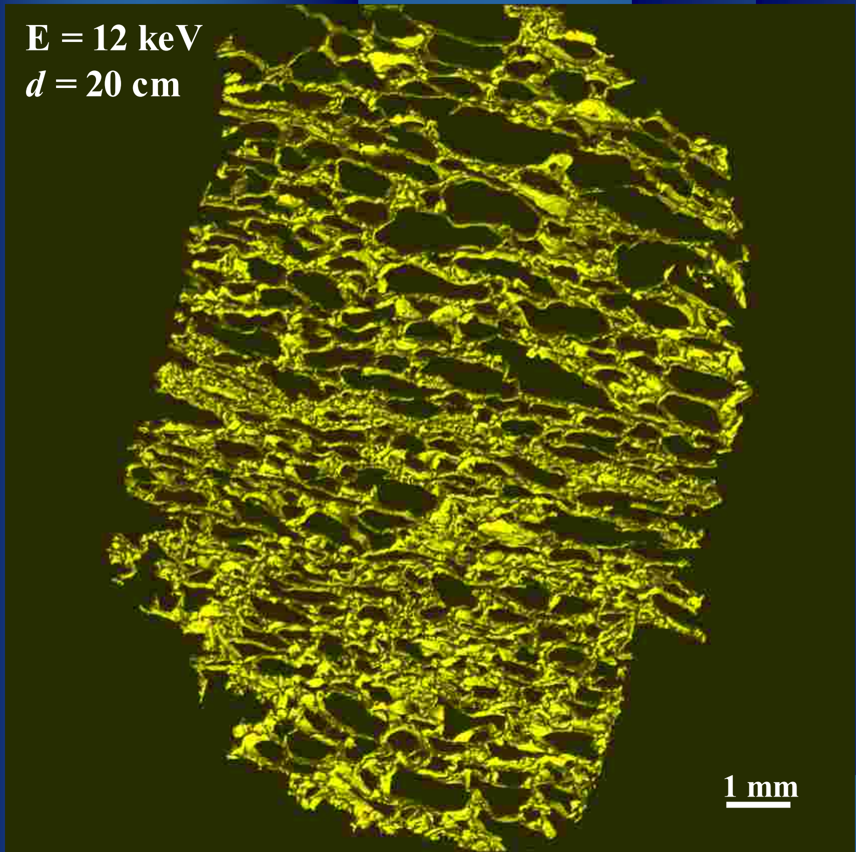

Aerated chocolate

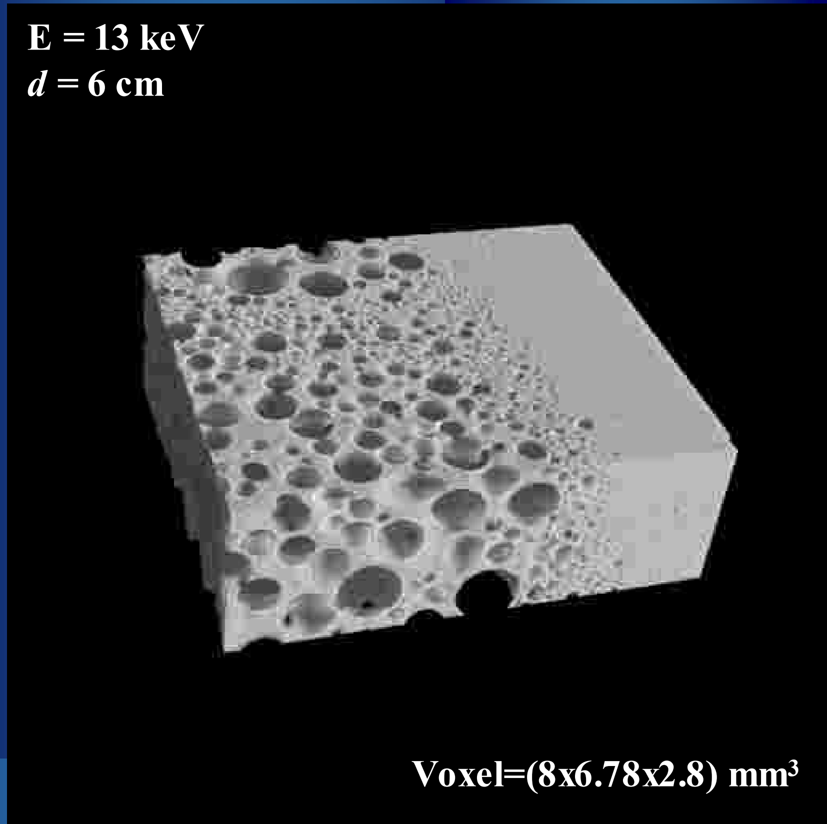

P.M. Falcone et al., Advances in Food and Nutrition Research 51 (2006), 205-263
P. M. Falcone et al., Journal of Food Science 69 (2004) E39-E43

Polymeric foams

Wood samples

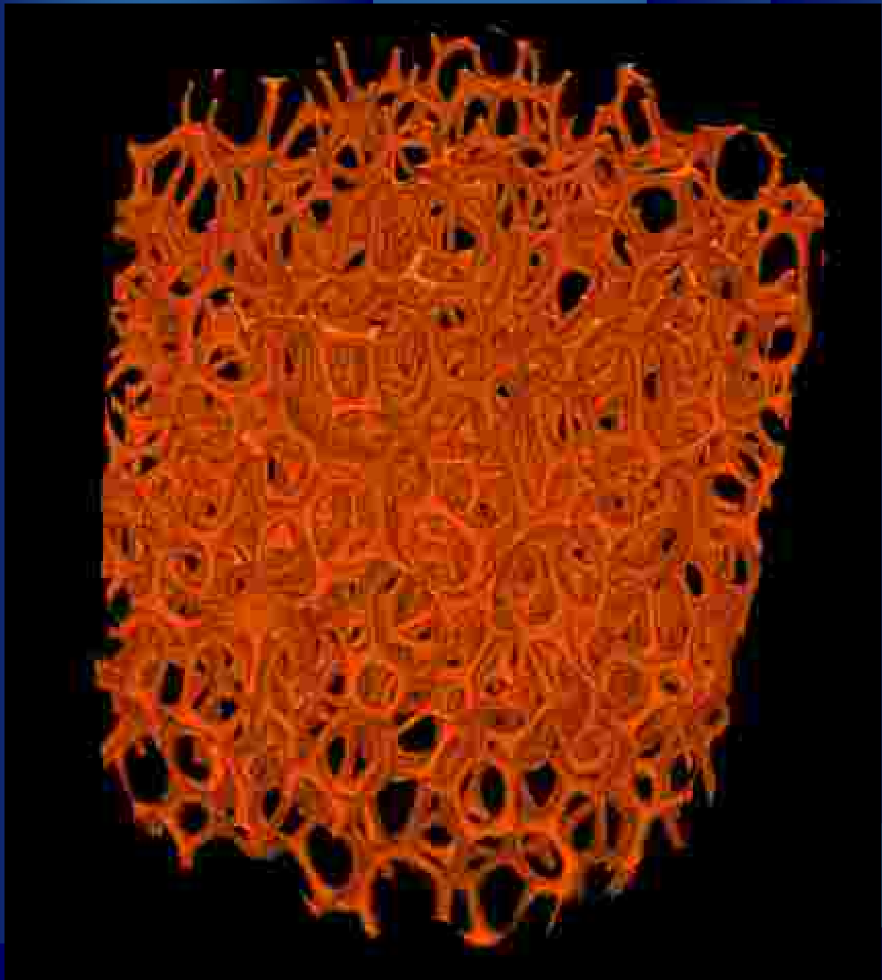

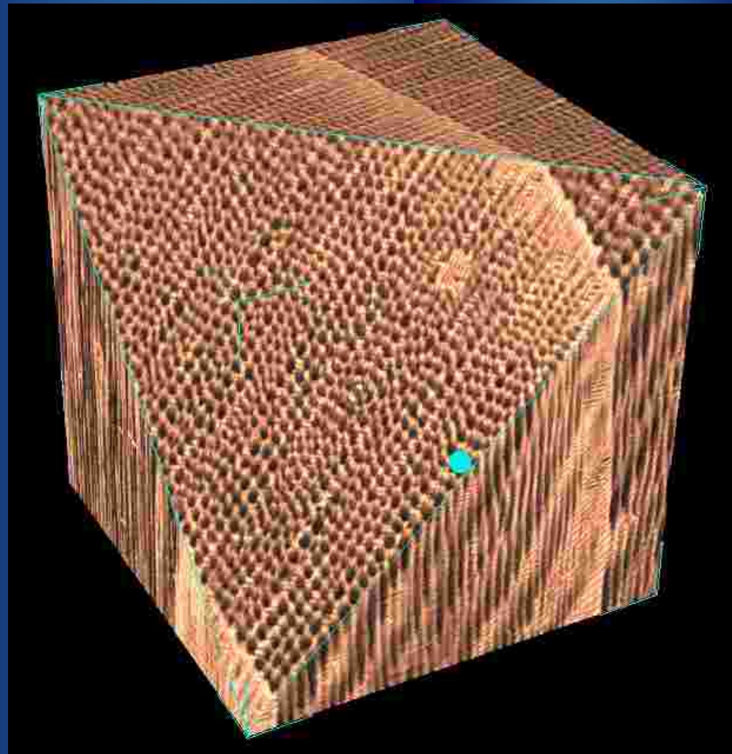

Courtesy of L. Bregant, Univ. of Trieste

D. Dreossi et al., in Wood Science for Conservation of Cultural Heritage - Florence 2007, Firenze University Press 2010, Florence (Italy), pp. 34-39

Kidney stones

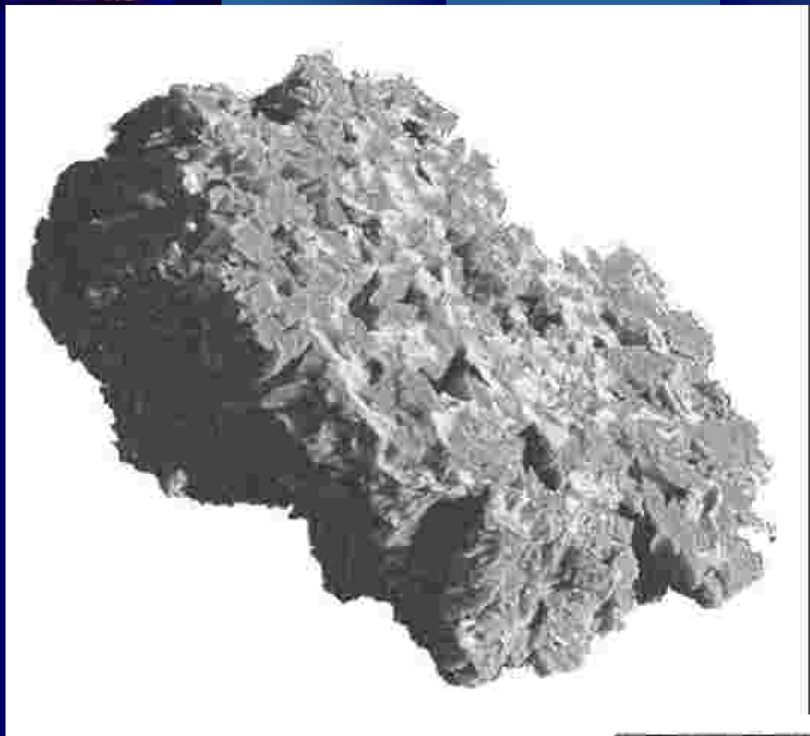

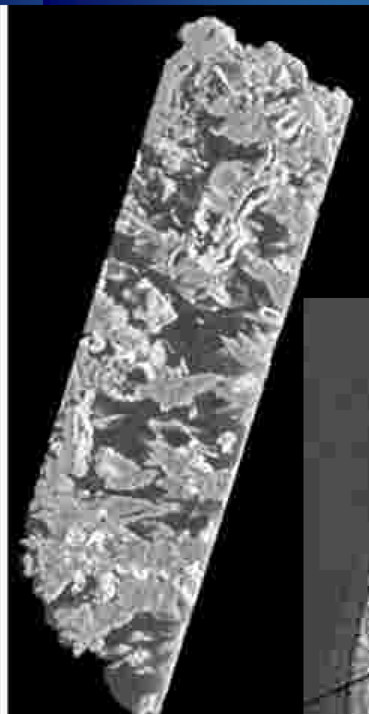

Cement-based materials

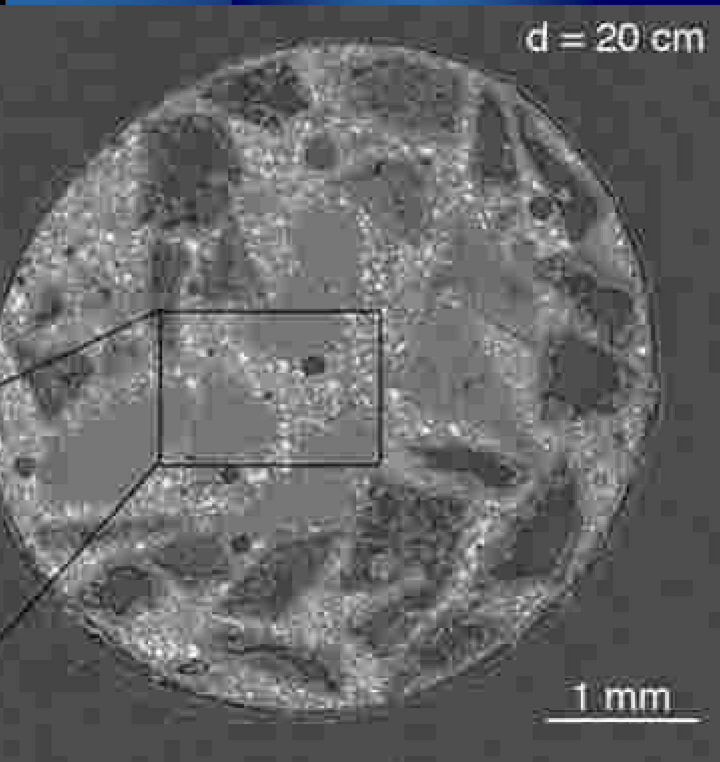

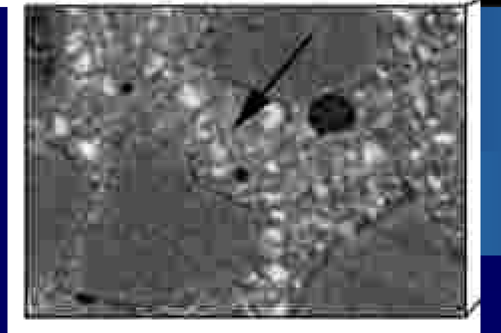

J. Kaiser et al., Urological Research, 39 (2011) 259-267.

N. Marinoni et al., Journal of Material Science, 44 (2009) 5815-5823

Analysis of a Neanderthal tooth

Volume rendering

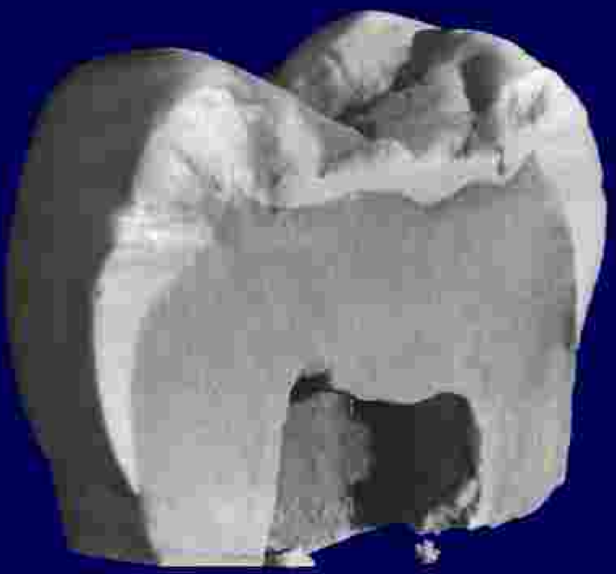

Volume: (1110 x 706 x 946) voxels^3
voxel side = 10 microns

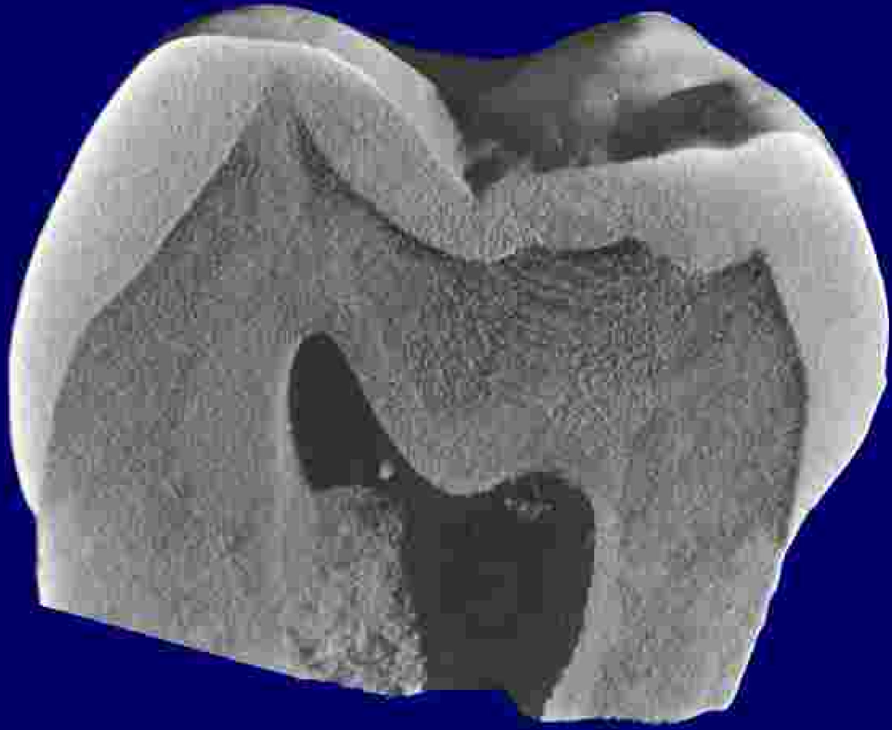

Courtesy of C. Tuniz

Fossil snake vertebra (1 Ma. old)

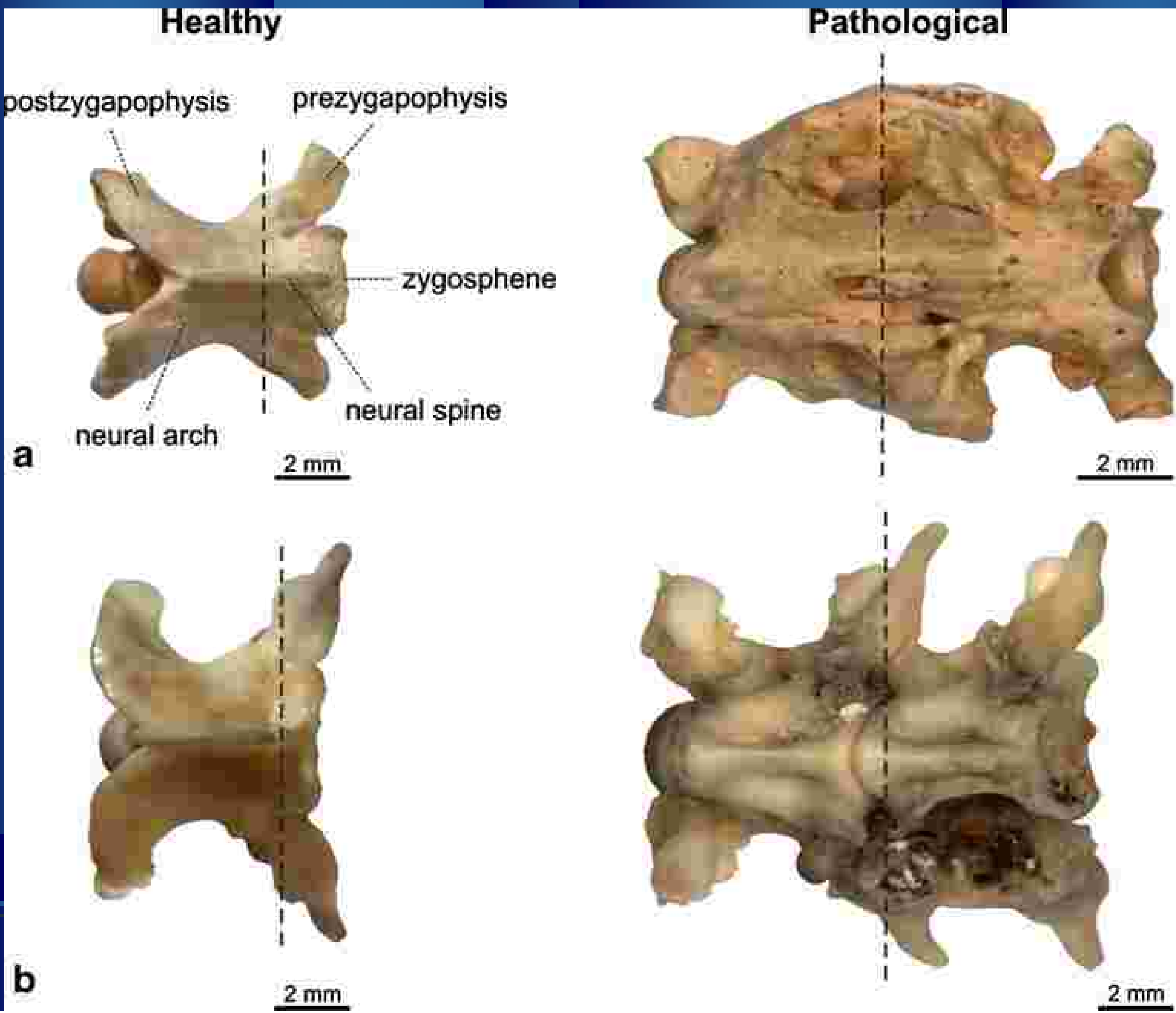

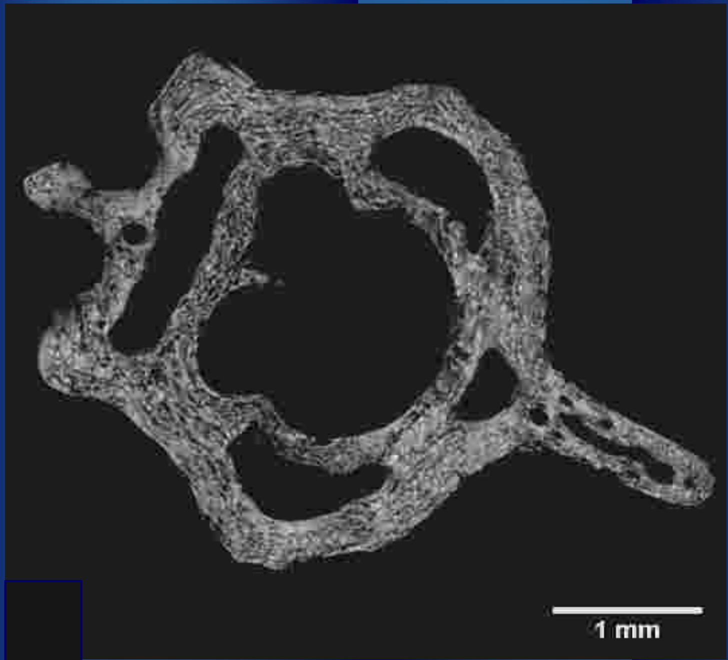

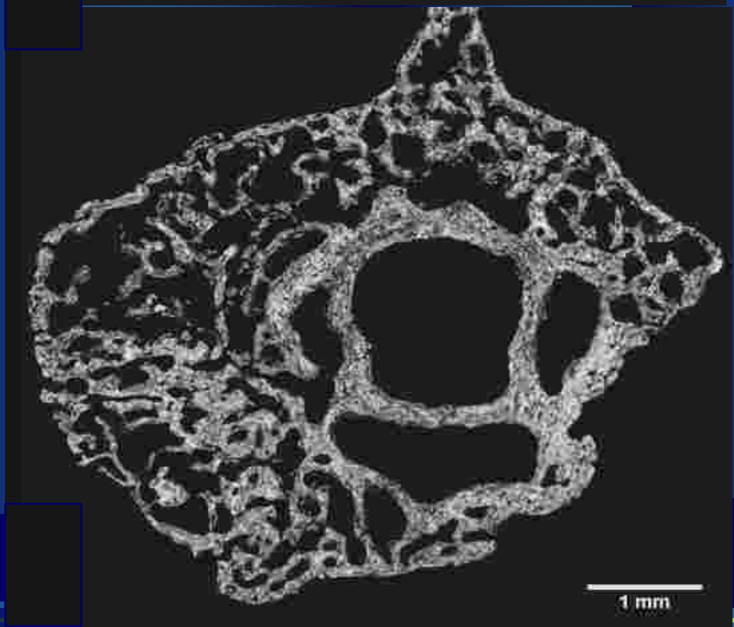

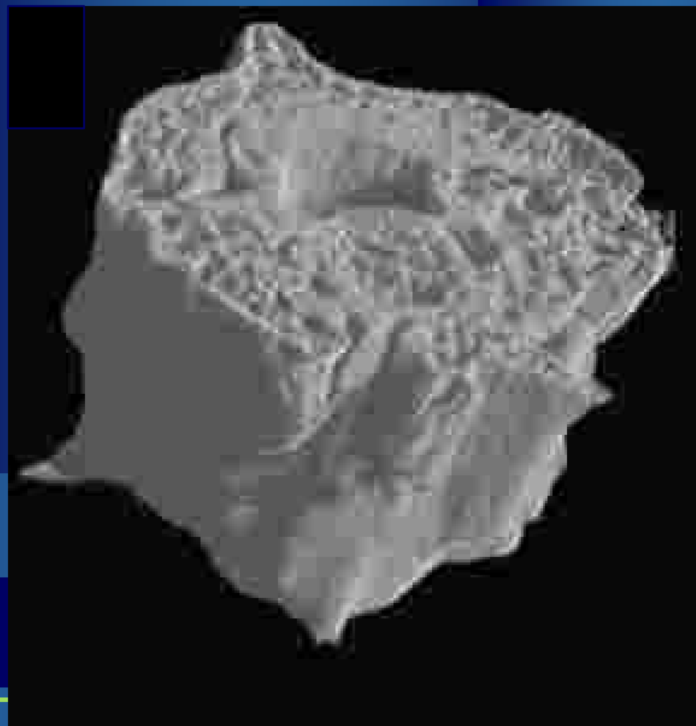

M. Galiová et al., Analytical and Bioanalytical Chemistry, 398 (2010) 1095-1107.

Healthy *Pathological*

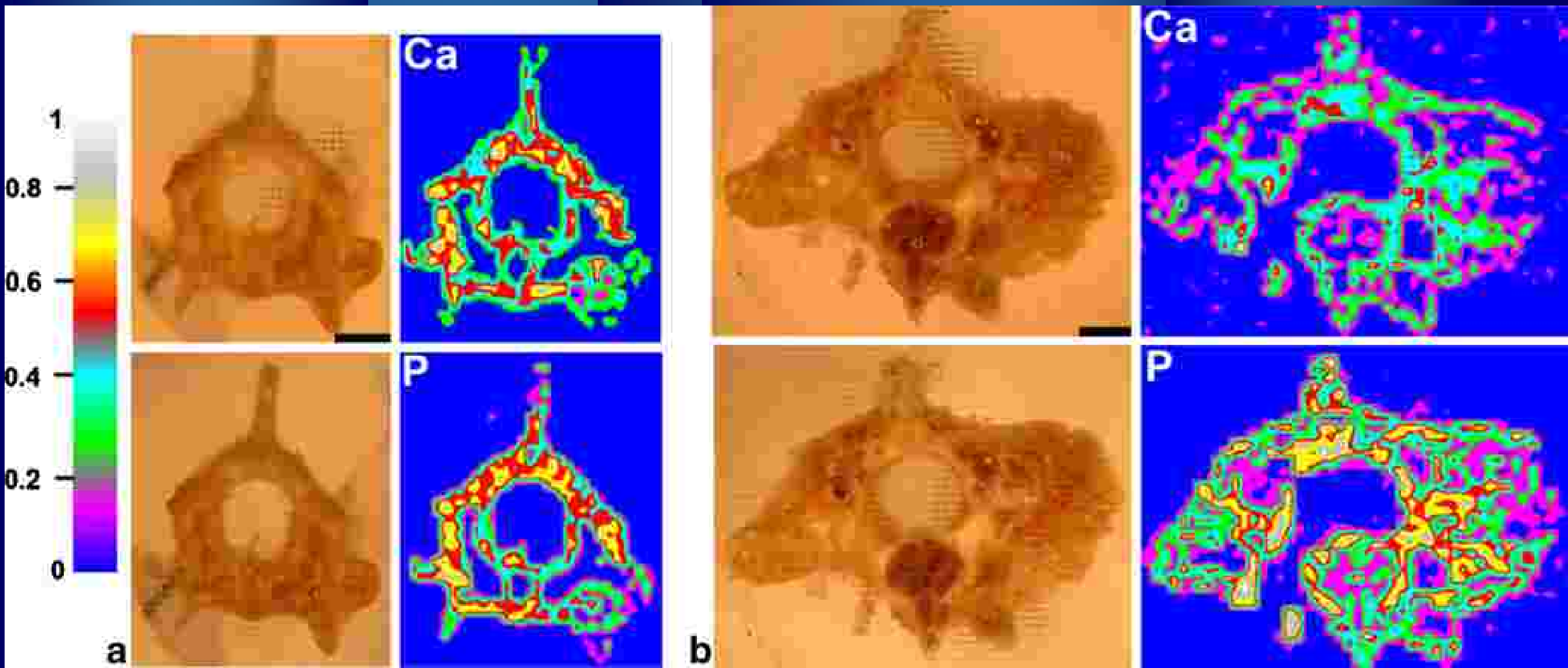

Spatial distribution of trace elements measured on fossil vertebra sections by DP-LIBS technique (bar length = 1 mm)

M. Galiová et al., Analytical and Bioanalytical Chemistry, 398 (2010) 1095-1107.

3D analysis of the canal network of Stylaster sp. (Cnidaria, Hydrozoa) by means of X-ray μCT

Colony *in situ*

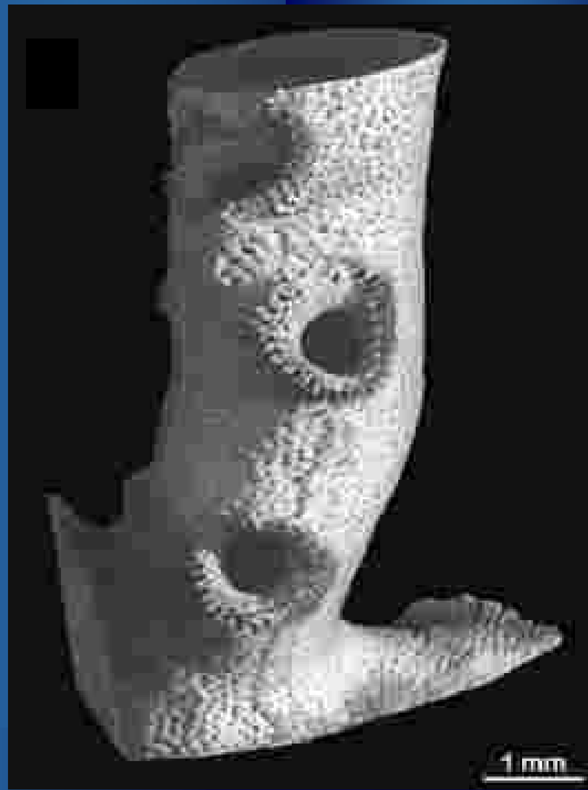

3D rendering of a branch

S. Puce et al., Zoomorphology, 130 (2011) 85-95.

Branch of the colony without coenostem

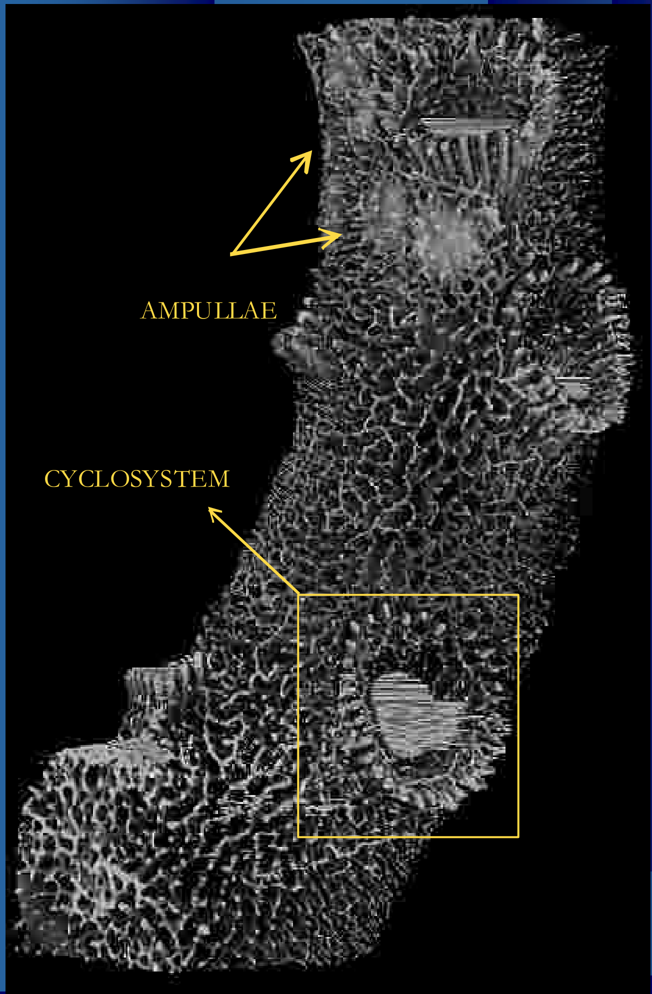

Section of the branch

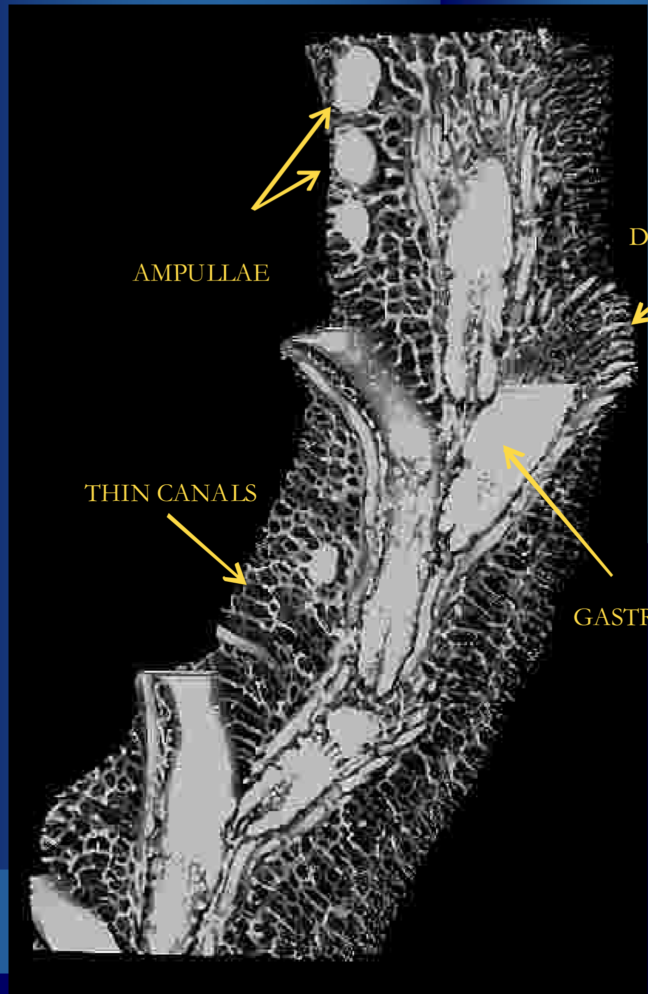

S. Puce et al., Zoomorphology, 130 (2011) 85-95.

Study of the growth process

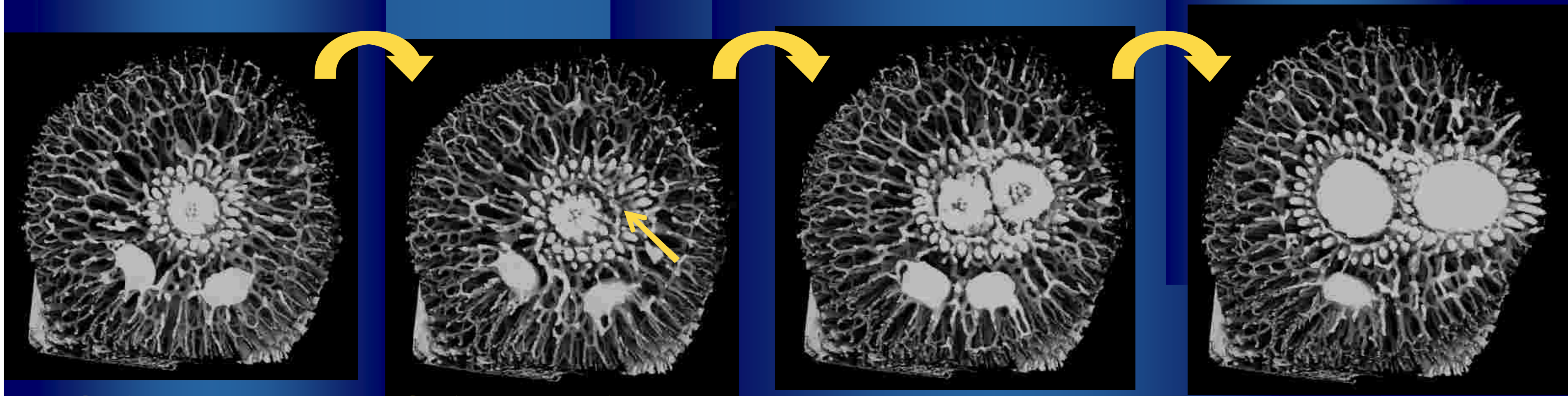

Cyclosystem

Cyclosystem enlargement

Old and new gastropores surrounded by a single ring of dactylopores

Cyclosystems completely separated

The analysis of a sequence of the coral's transverse sections revealed the reciprocal relationship between adjacent cyclosystems: each new cyclosystem appears to bud between the gastropore and the dactylopores of the last formed one.

University of Bologna
Physics Department

ISTITUTI ORTOPEDICI RIZZOLI

eletrra

ISTITUTI ORTOPEDICI RIZZOLI

elettra

10 cm

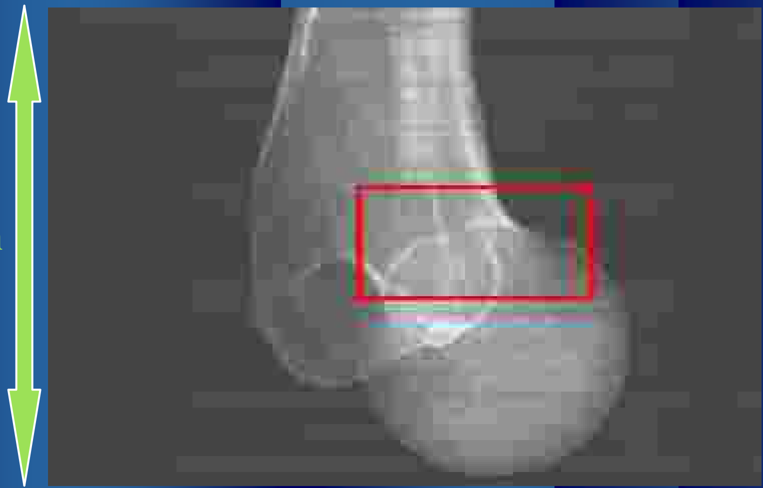

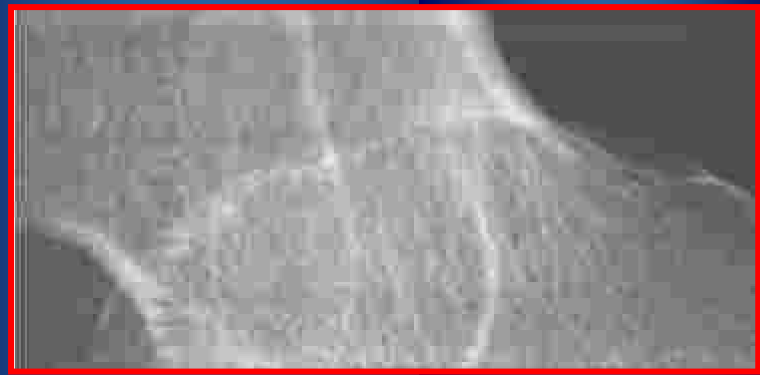

E = 34 keV

t_{exp} = 600 sec

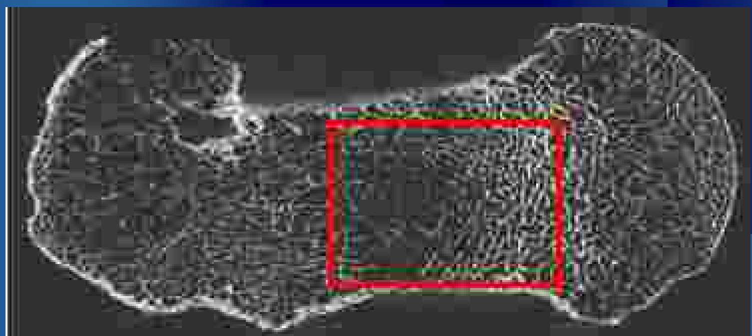

Reconstructed slice

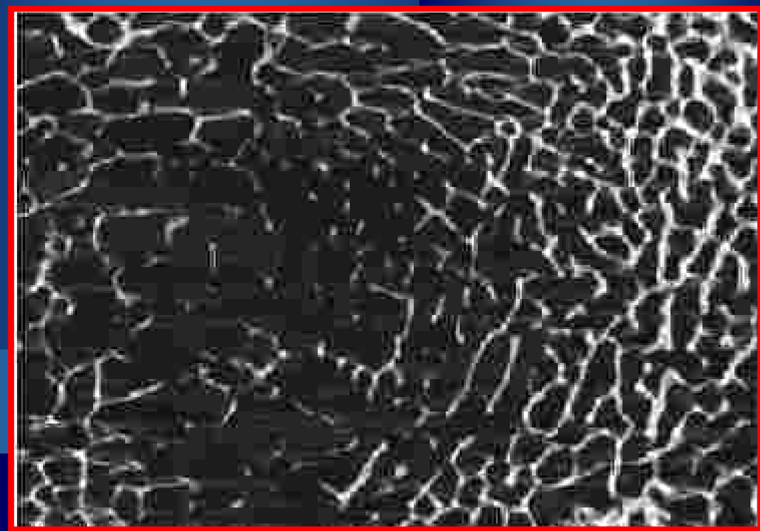

F. Baruffaldi et al., IEEE Transactions on Nuclear Science 53, No 5 (2006), 2584-2590.

ISTITUTI ORTOPEDICI RIZZOLI

F. Baruffaldi, M. Bettuzzi, D. Bianconi, R. Brancaccio, S. Cornacchia, N. Lanconelli, L. Mancini, M. P. Morigi, A. Pasini, E. Perilli, D. Romani, A. Rossi, F. Casali

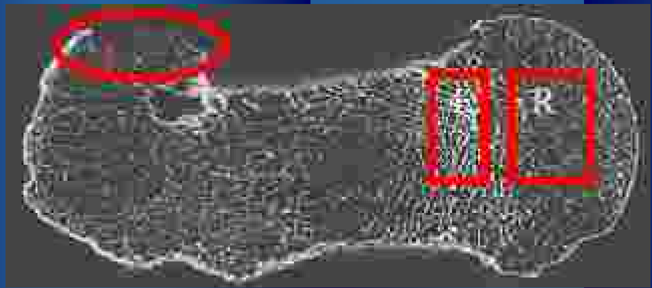

	BV/TV [%]	Tb.Th [µm]	Tb.N [mm^{-1}]	Tb.Sp [µm]
Left ROI	21.4±0.3	167±2	1.28±0.03	610±20
Right ROI	13.8±0.2	120±1	1.17±0.02	740±10

	BV/TV [%]	Tb.Th [µm]	Tb.N [mm^{-1}]	Tb.Sp [µm]
Big ROI	17.5±0.2	122±2	1.44±0.02	576±8

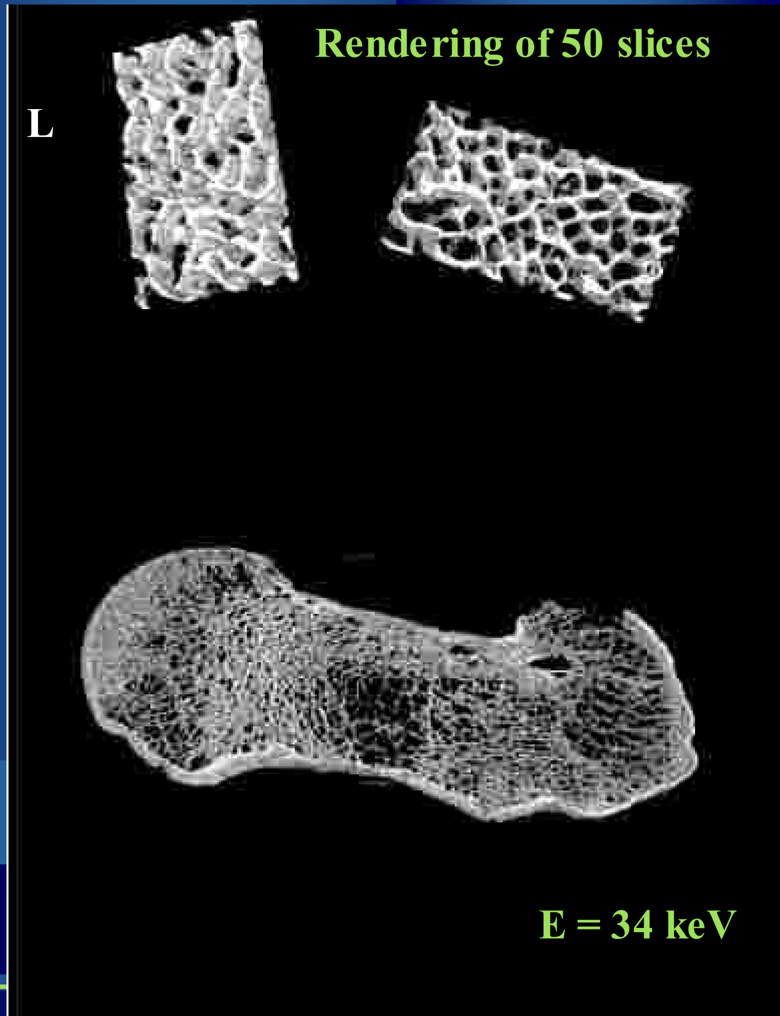

F. Baruffaldi et al., IEEE Transactions on Nuclear Science 53, No 5 (2006), 2584-2590.

Original waterlogged glass, completely corroded

Fragment provided by the Museum of London

E = 25 keV ***d*** **= 66 cm;** ***acquisition time: 4h***

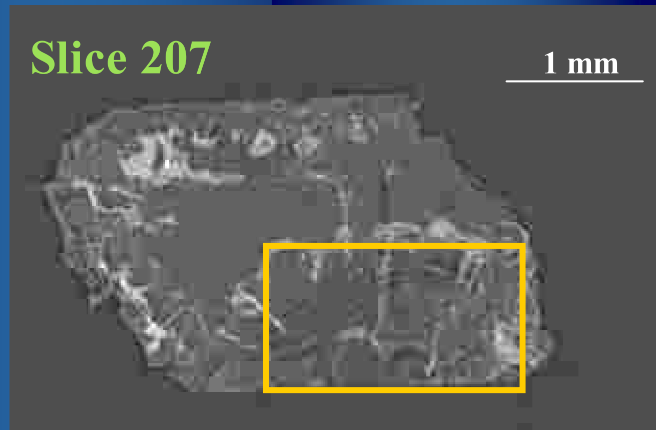

Cine rendering of channels
(9.0 x 9.0 x 0.2) mm^3

It is possible to visualize:

→ the gel-layer channels

→ the lamellar structure inside the corroded glass

L. Mancini et al., Journal of Neutron Research 14, No. 1 (2006) 75–79.

Model glasses covered by a polymeric layer

Bulk polymers (acrylates) are used as consolidant materials

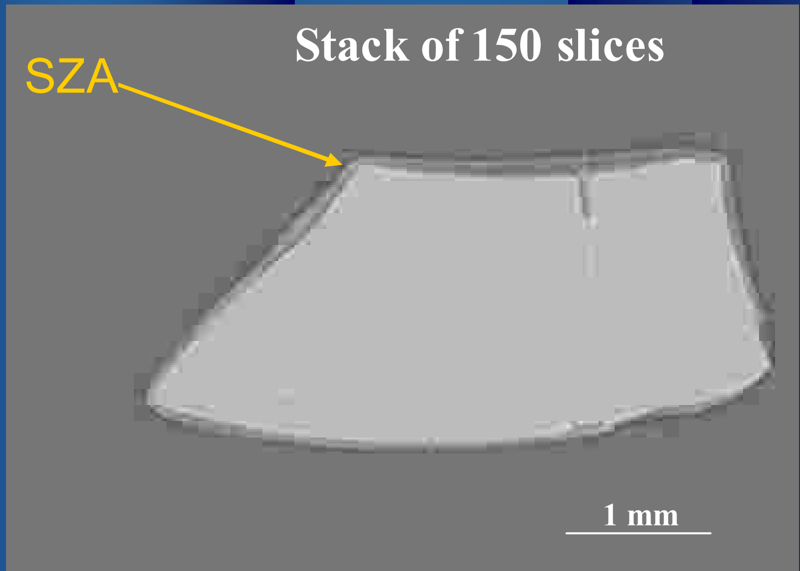

Inorganic layer based on Silicium-Zirconium-Alcoxides (SZA) well visible on the glass surfaceS. SZA penetrates the crack on the upper surface. The channel is completely filled without formation of voids.

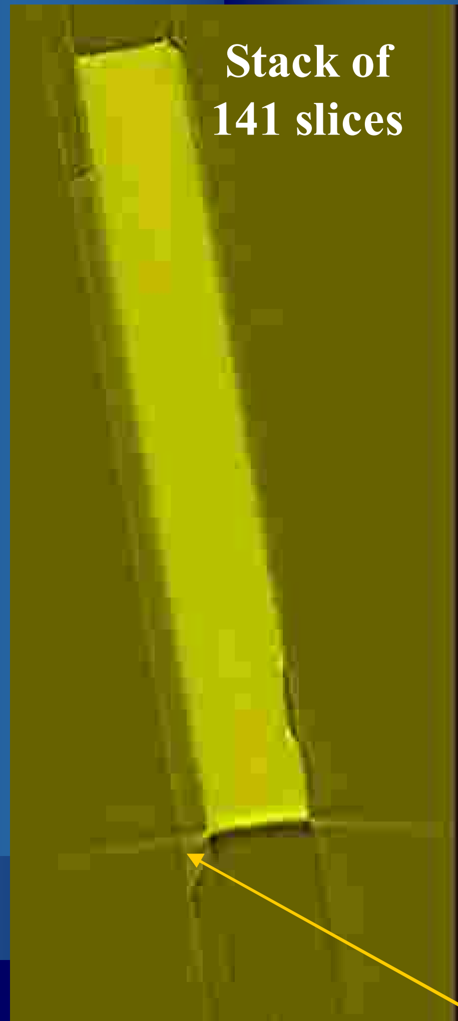

A 200 μm layer of Araldite well visible.

E = 25 keV, *d* = 66 cm

Gerlach S. et al., Elettra Highlights 2003, 80

Non-destructive evaluation of musical instruments

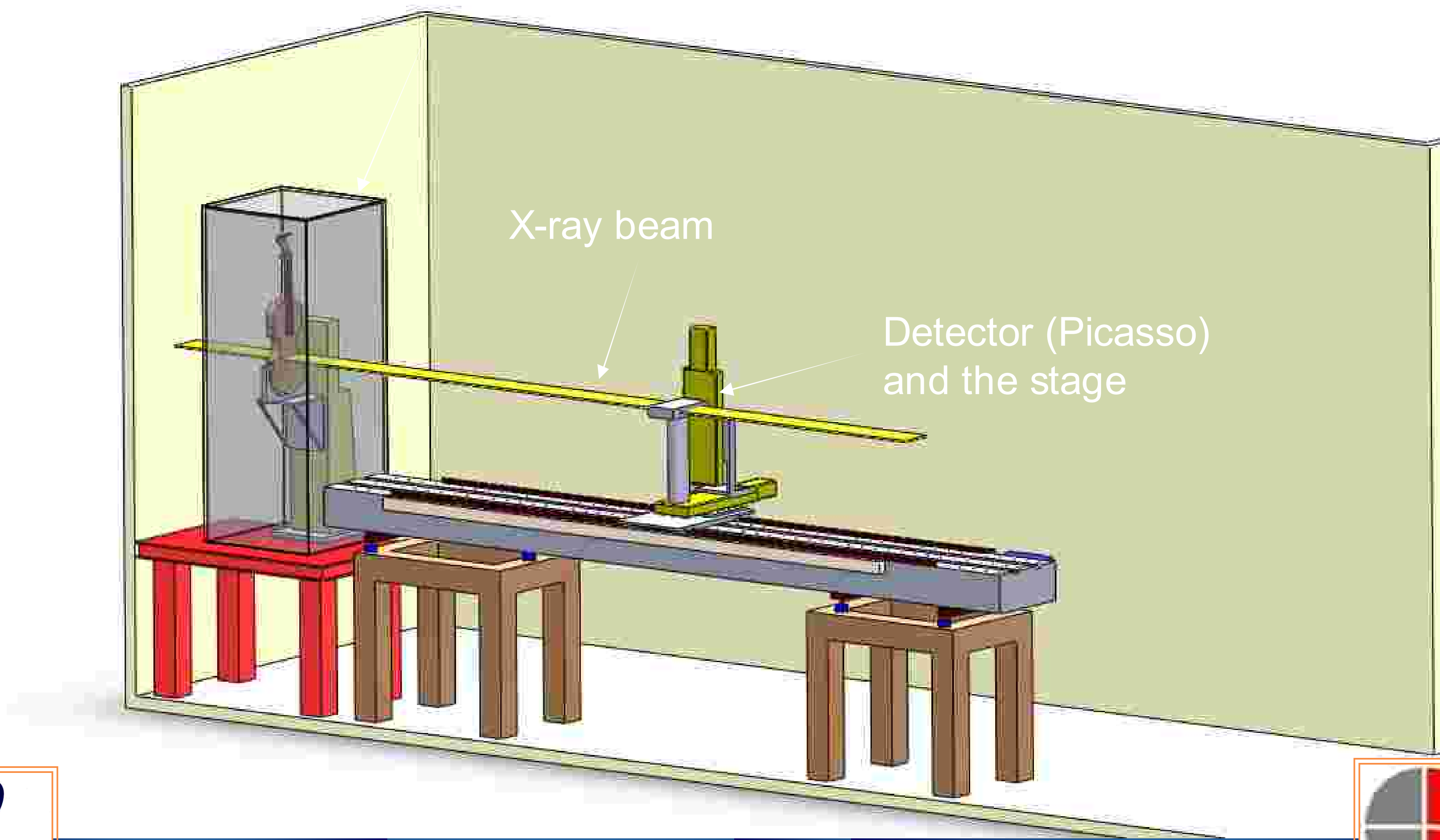

Non-destructive evaluation of musical instruments

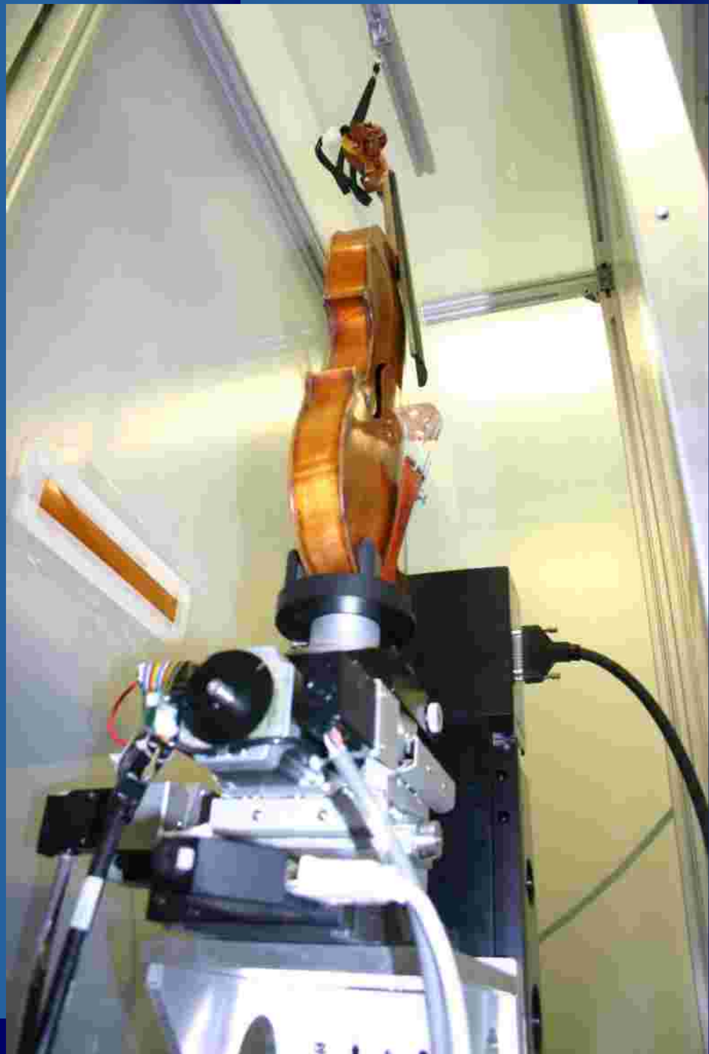

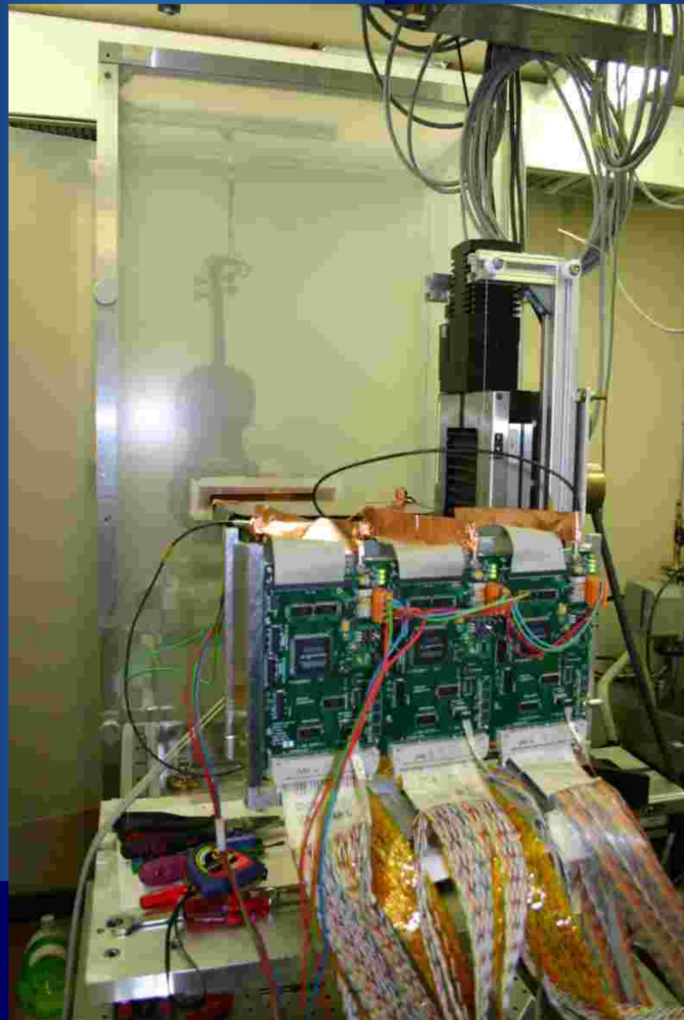

State-of-the-art clinical instrument of the Azienda Ospedaliera – University of Trieste

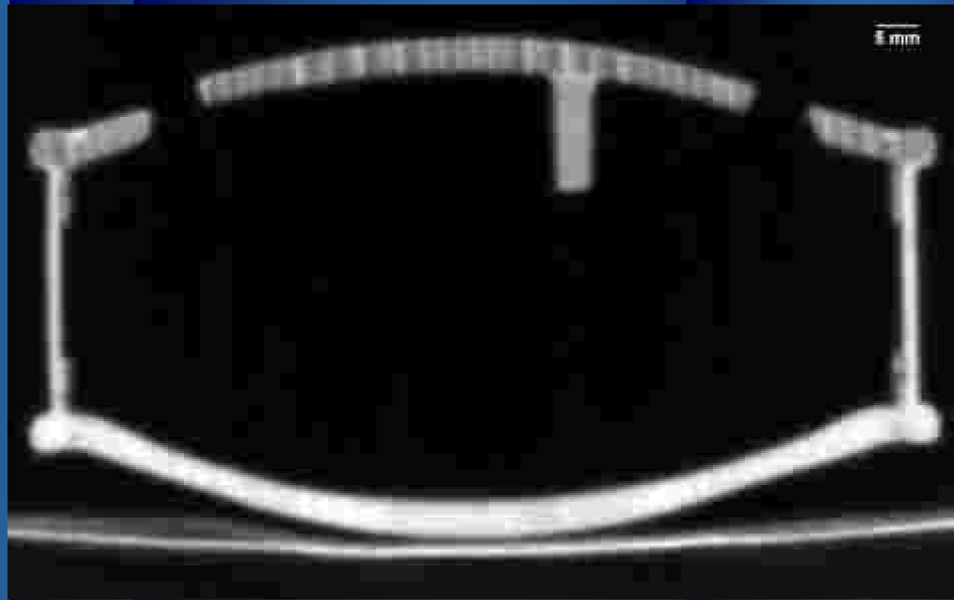

SYRMEP

L. Rigon et al., e-Preservation Science, 7 (2010) 71-77.

SYRMEP: details

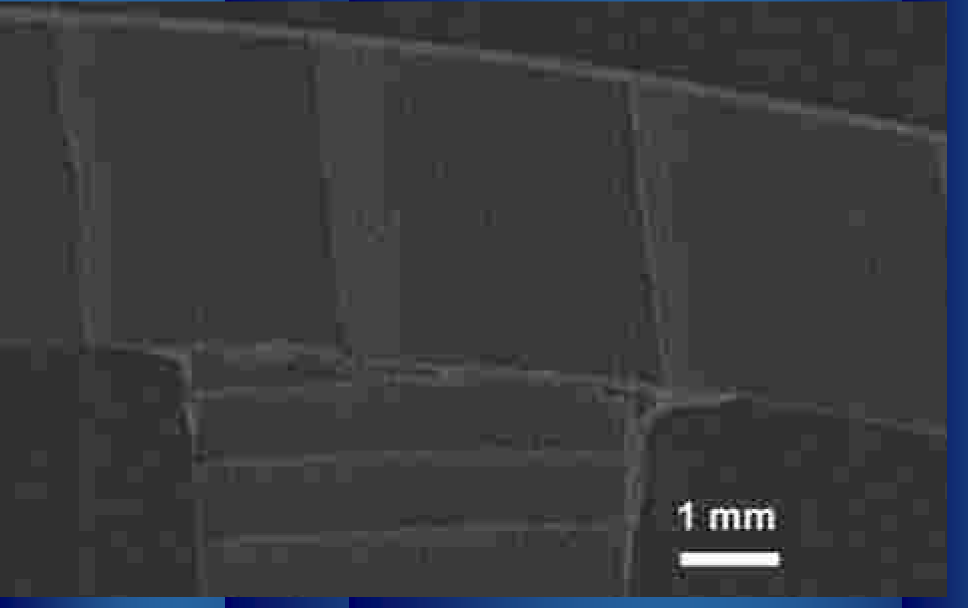

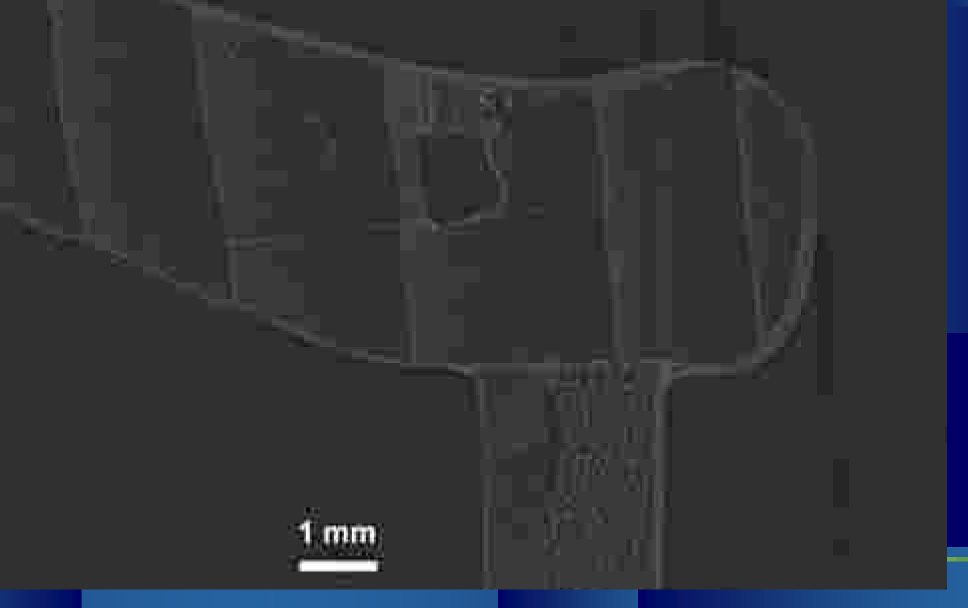

L. Rigon et al., e-Preservation Science, 7 (2010) 71-77.

μ–CT of the organ by Lorenzo da Pavia

- **Portable organ constructed in 1494 (Museo Correr of Venezia, Italy)**
- **Instrument of great historical and artistic relevance**
- **Pipes made with rolled and glued cardboard**
- **Structural characterization of the paper pipes to define strategies for restoration, conservation and possible substitution**

http://www.lombardia.beniculturali.it/

Virtual slice of a paper pipe

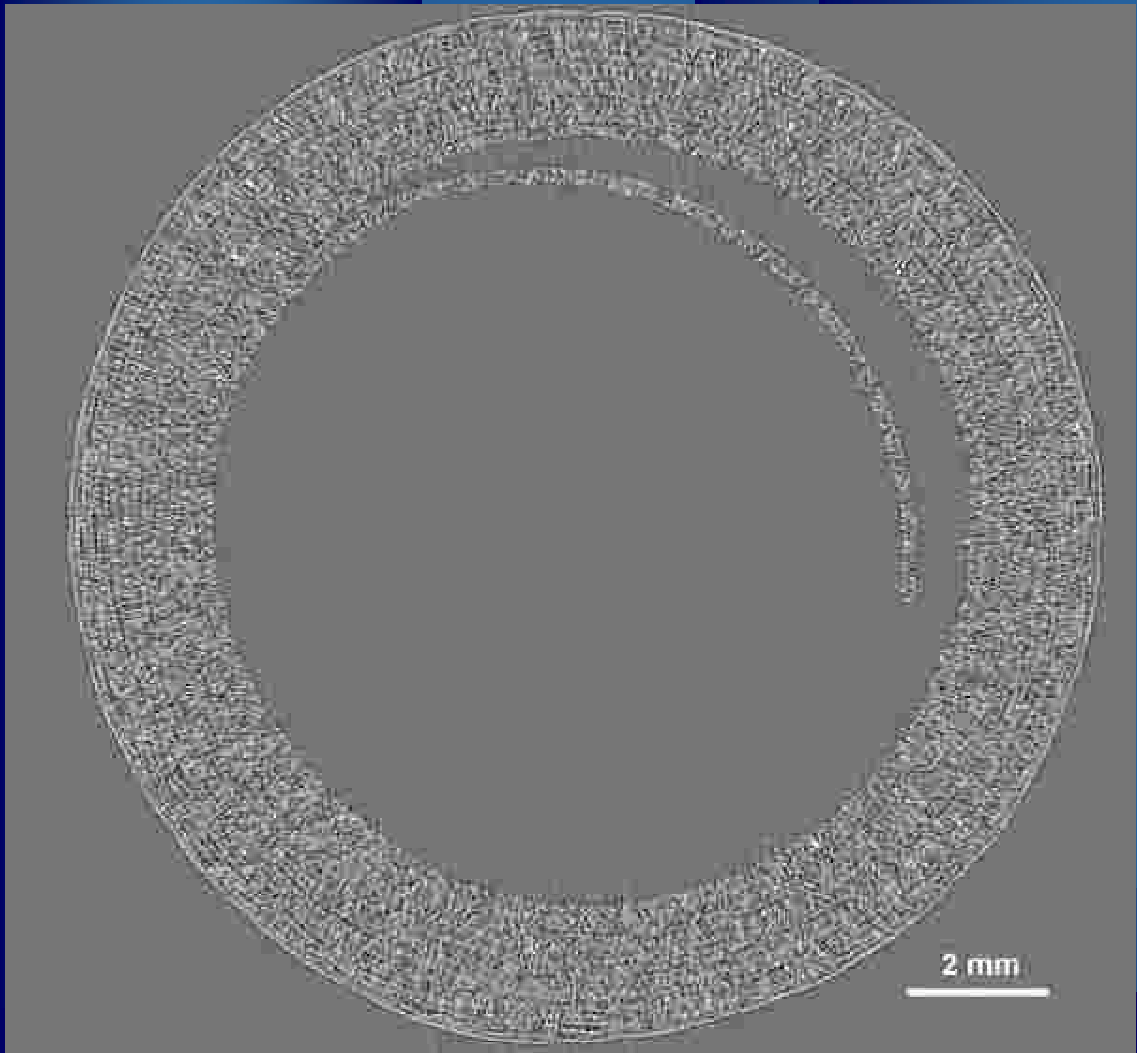

- 10 layers 0.25 mm thick
- good quality of external layer
- good adhesion of layers, except the inner one

Energy = 19 keV, Num. proj = 1440, D = 300 mm
exp. time = 1 sec, voxel size = 9 µm

Slice at the wood foot position

- 10 layers 0.25 mm thick
- good quality of the external layer
- evident degradation of the layers adhesion

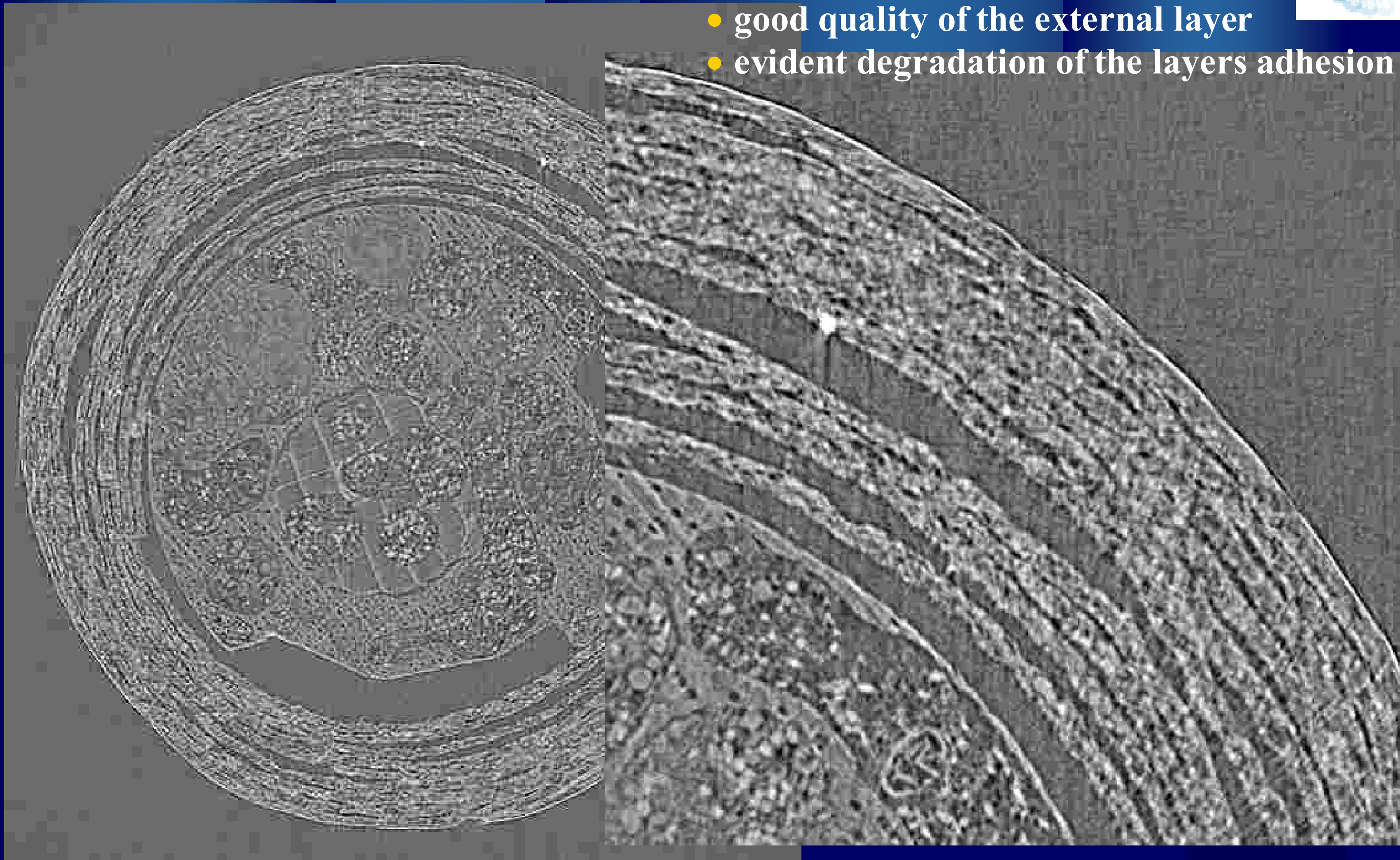

Energy = 23 keV, Num. proj = 1440, D = 300 mm
exp. time = 1 sec, voxel size = 9 µm

- presence of larvae
- possibility of wood species characterization

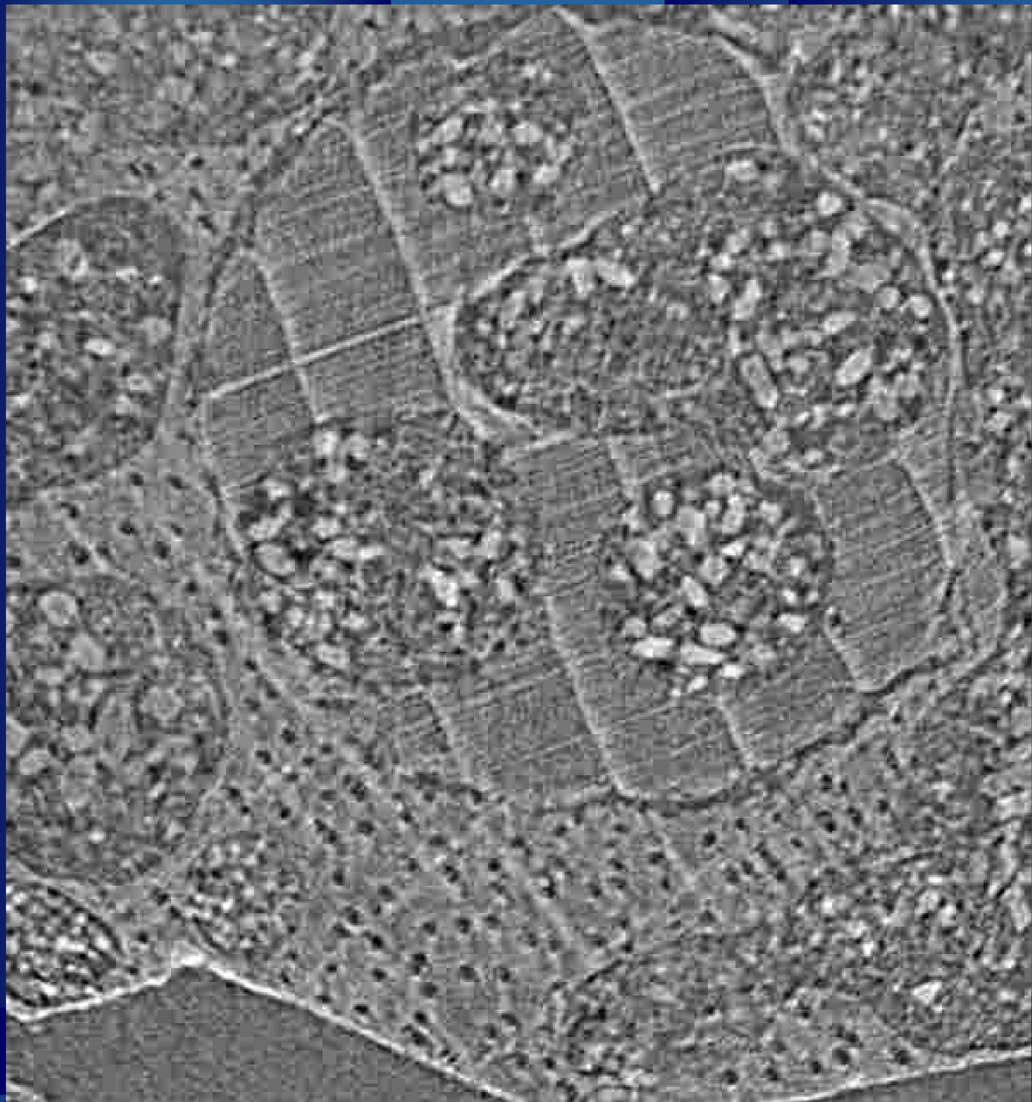

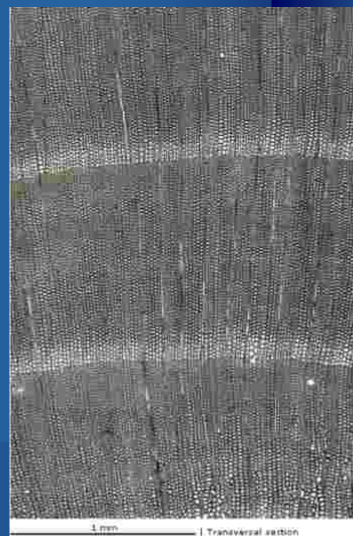

Picea abies

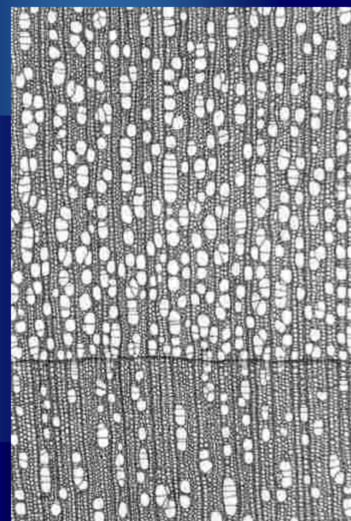

Alnus glutinosa

Why the Pore3D project?

- A sw library specifically designed for ***X-ray -CT images*** of porous media and multiphase systems, Manipulation of ***huge datasets*** with ***common hw***.

- ***Different strategies of analysis*** as a function of the scientific application: *Pore3D* implements ***several algorithms for each step*** of the analysis, having ***a full control of the parameters*** of the algorithm and of the intermediate results.

- On the basis of ***specific know-how*** of the ***SYRMEP collaboration*** the main aim was to merge many of features implemented in existing software, in some cases customizing it or adding new tools.

Pore3D is a software tool for **3D image processing** and **analysis**

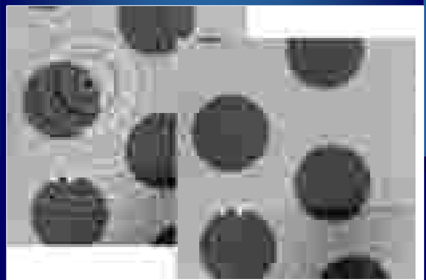

Filters
Basic (mean, median, gaussian, ...)
Anisotropic diffusion
Bilateral
Ring artifacts reduction
Binary (median, clear border, ...)

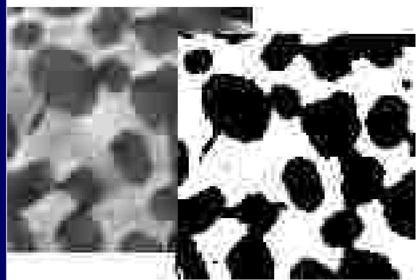

Segmentation
Automatic thresholding (Otsu, Kittler, ...)
Adaptive thresholding
Region growing
Multiphase thresholding
Clustering (*k*-means, *k*-medians, ...)

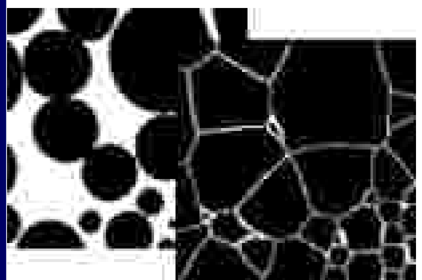

Morphological processing
Dilation and erosion
Morphological reconstruction
Watershed segmentation
Distance transform
H-Minima filter

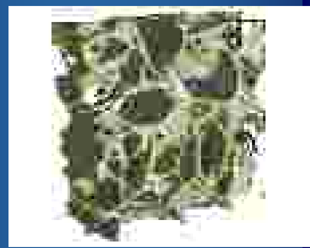

Skeleton extraction
Thinning
Medial axis (LKC)
DOHT
Gradient Vector Flow
Skeleton pruning
Skeleton labeling

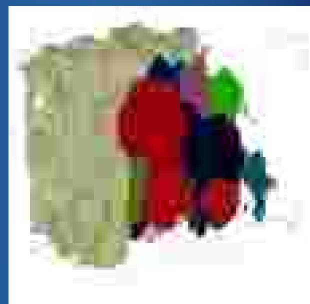

Analysis
Minkowski functionals
Morphometric analysis
Anisotropy analysis
Blob analysis
Skeleton analysis
Textural analysis (fractal dimension, ...)

http://ulisse.elettra.trieste.it/uos/pore3d

F. Brun et al., NIM A, 615 (2010) 326–332

Analysis of human kidney stones

11847	Crop_1	Crop_2	Whole stack	IRS results
Whewellite (%)	15.9	15.2	14.9	20
Weddellite (%)	50.5	51.1	52.7	45
Apatite (%)	33.6	33.7	32.4	35

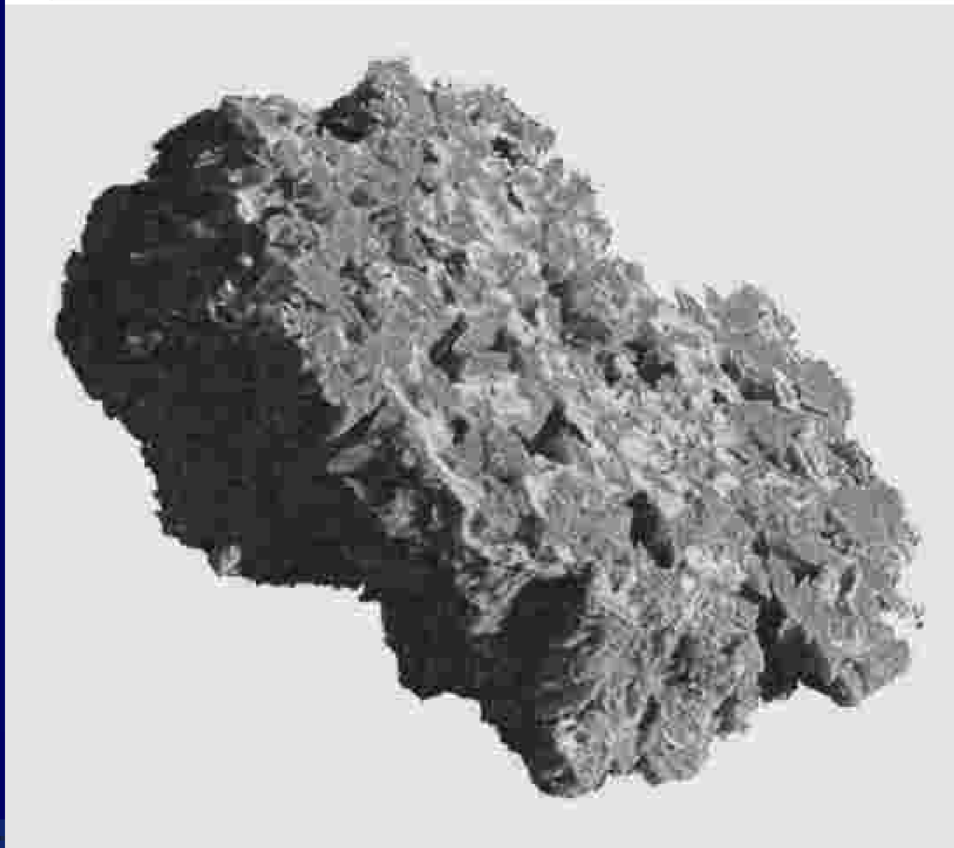

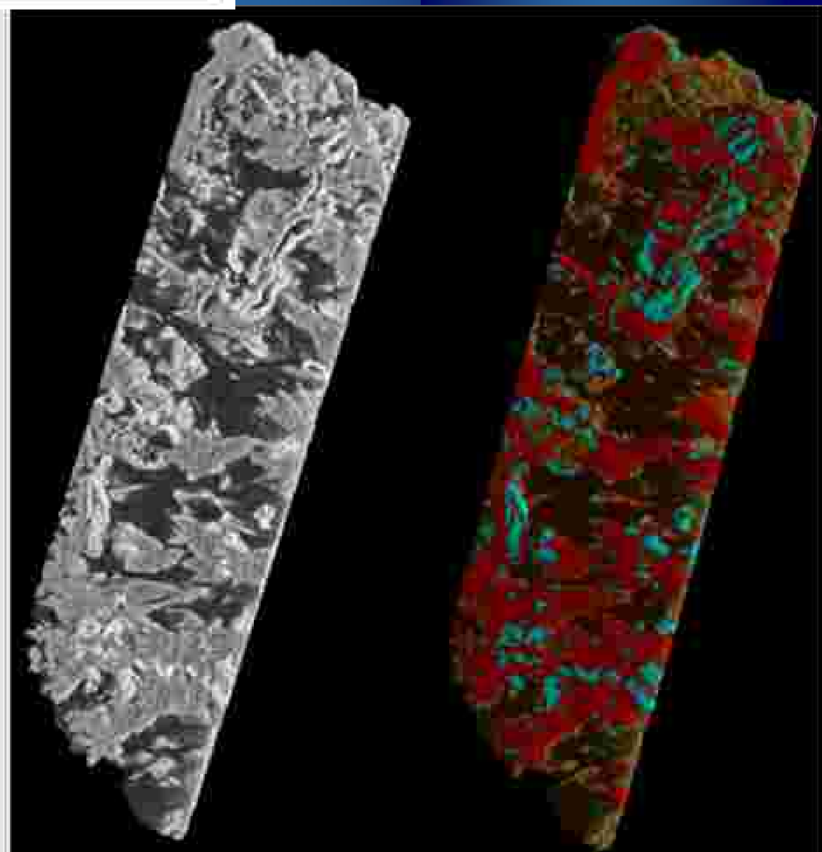

J. Kaiser et al., Urological Research, 39 (2011) 259-267.

Volcanic rocks

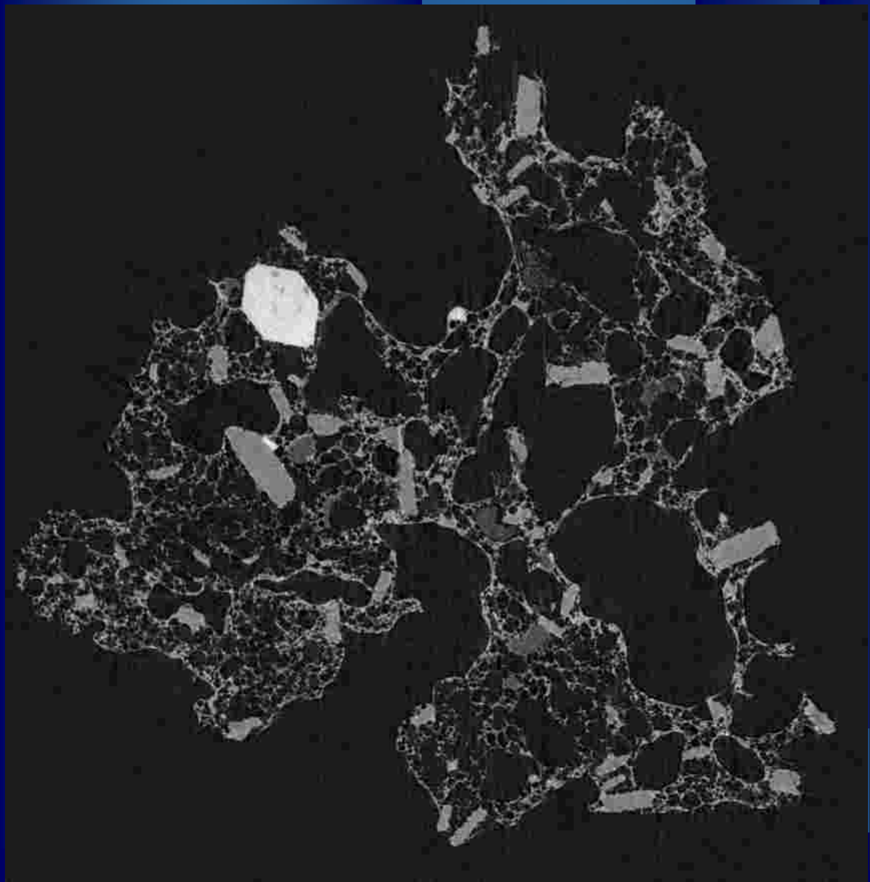

Courtesy of M. Polacci

Scoria from Ambryn, vesiculated, low crystallized

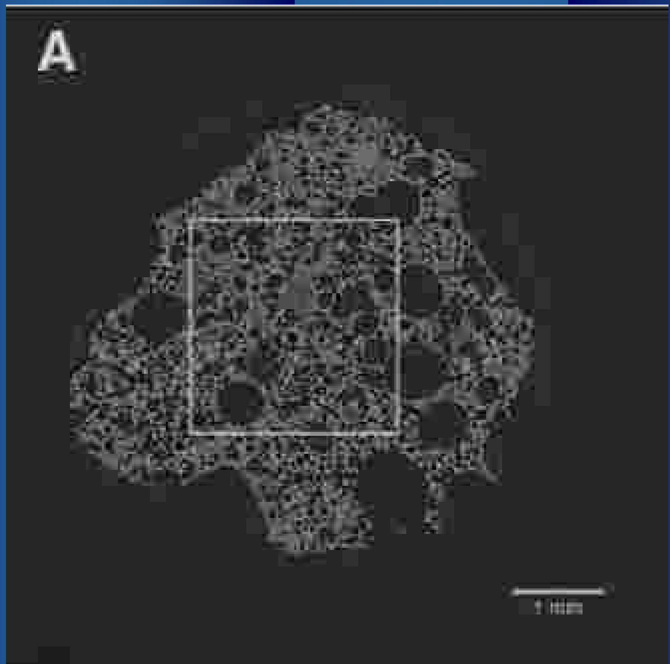

Abundance of isolated vesicles

Vesicles colored after connected component analysis.

Red: connected component

Yellow: the others

Vesicles isolated after watershed segmentation and border cleaning.

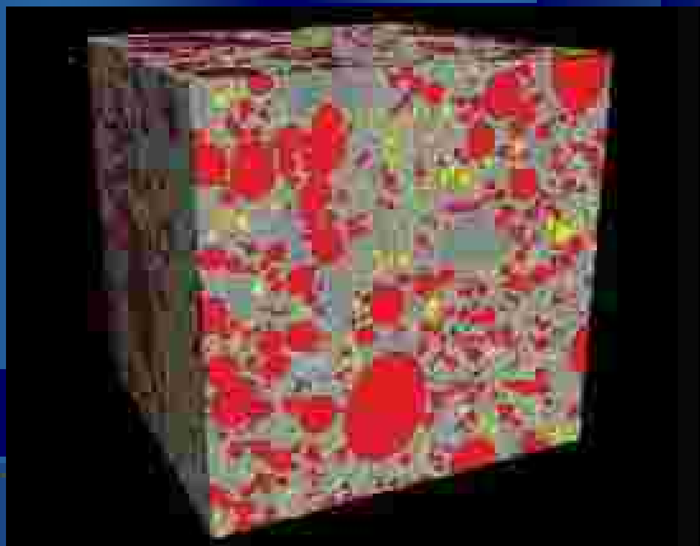

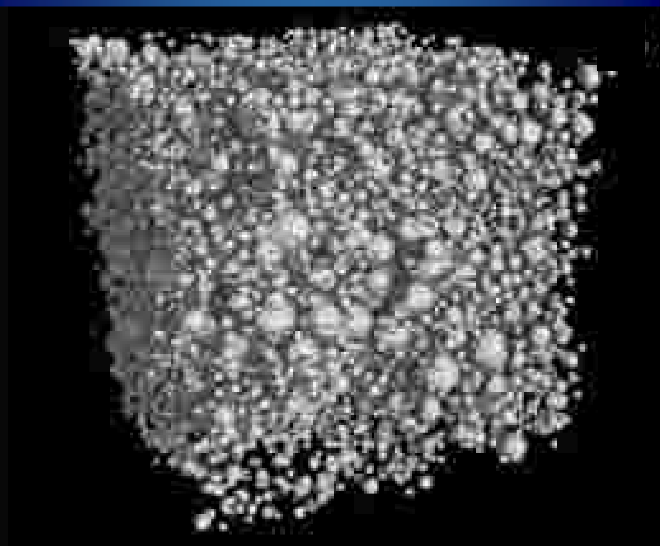

Pumice from Stromboli, highly vesiculated, low crystallized

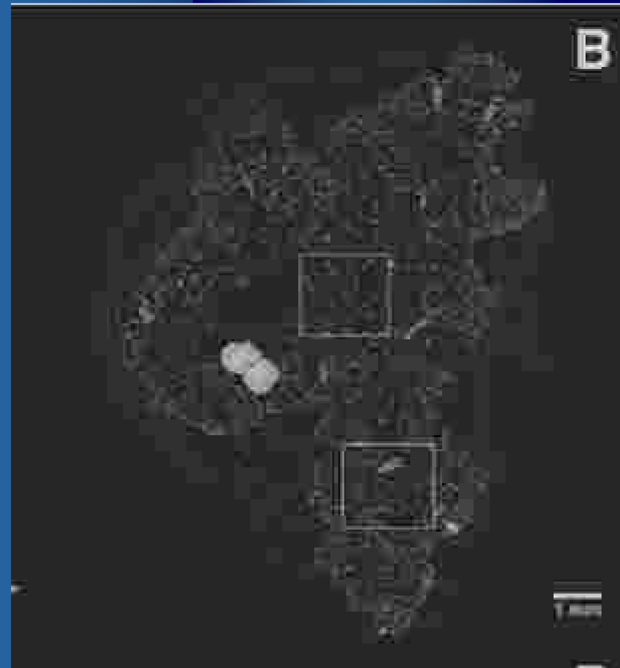

Vesicles coalesce in isotropic aggregates

Skeletonization of the porous phase

Red dots: skeleton nodes
Yellow lines: node-to-node branches

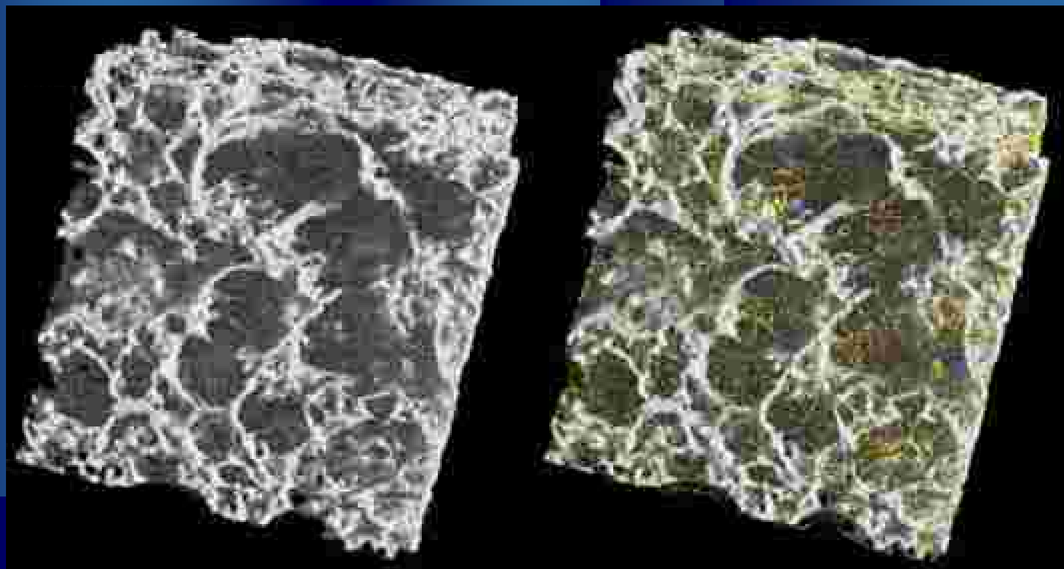

Quantification of degree of vesicle interconnectivity

D. Zandomeneghi et al., Geosphere, 6 (2010) 793-804

Scoria from Stromboli, poorly to moderately vesiculated, highly crystallized

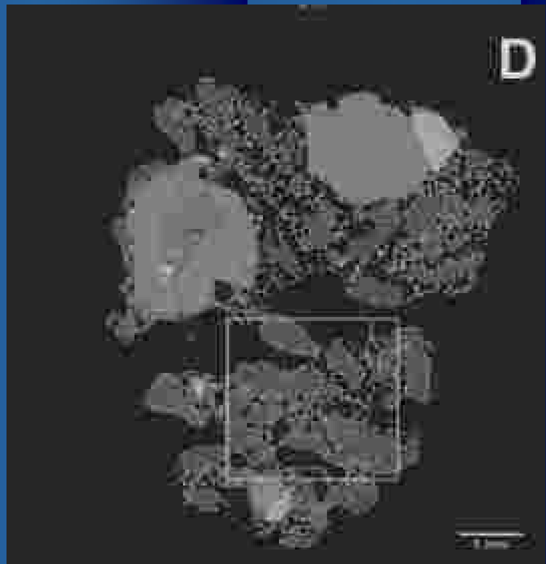

Blue: pyroxene crystals
Yellow: feldspar crystals
vesicles -> 36 %
pyroxenes -> 28%
feldspars -> 12%,

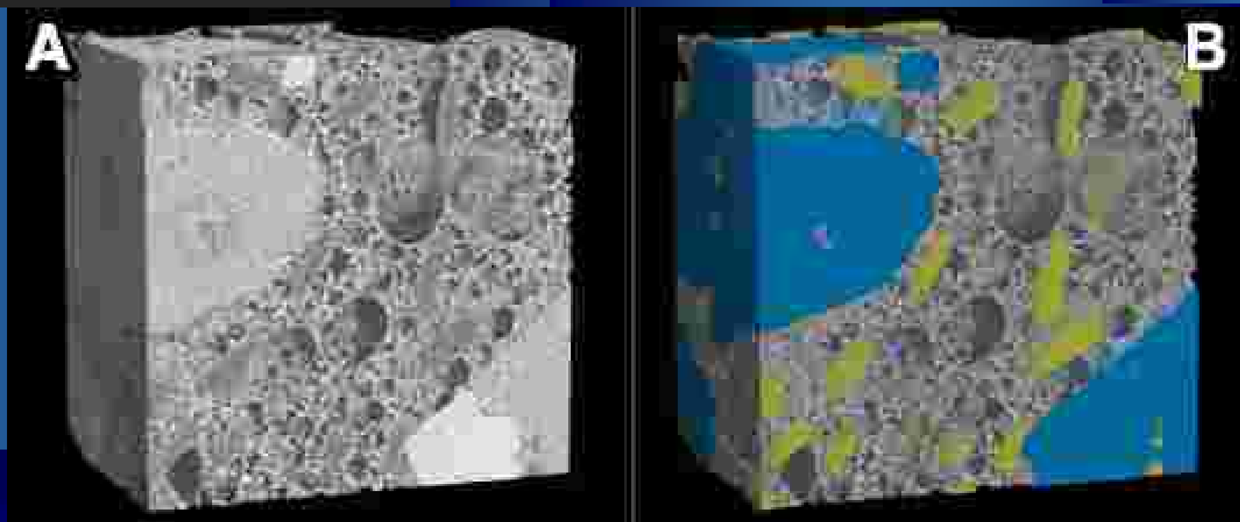

D. Zandomeneghi et al., Geosphere, 6 (2010) 793-804

Scoria from Etna (experiments performed at the TOMCAT beamline at the Swiss Synchrotron Light Source, PSI)

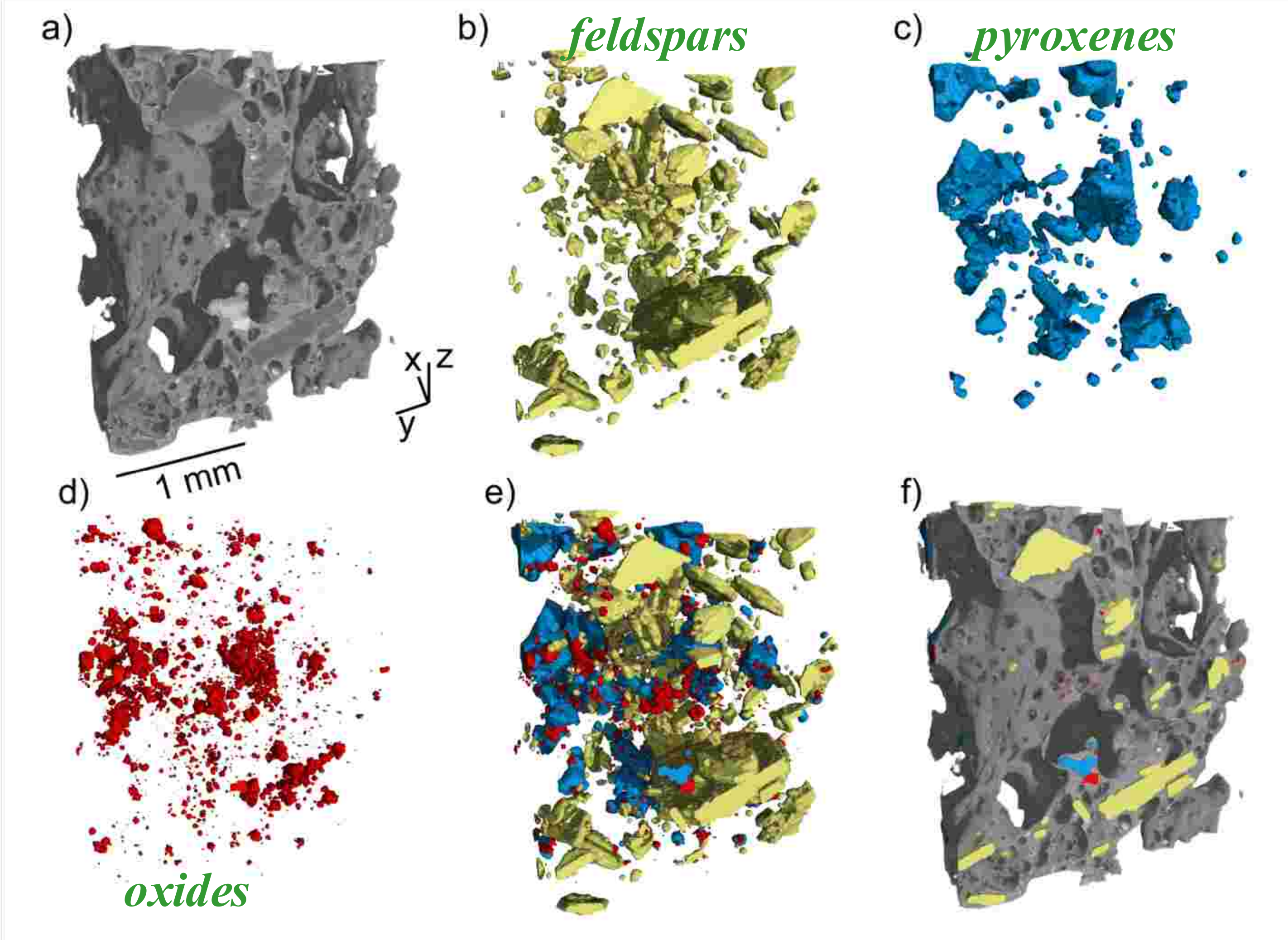

voxel size: 1.85 m

vesicles -> 68.9%, plagioclases -> 4.3%, pyroxenes -> 3.2%, "oxides" -> 0.7%, glass -> 22.9%.

M. Voltolini et al., J. of Volc. and Geothermal Res., 202 (2011) 83-95

elettra

Computed parameters by Pore3D

	STR1 scoria	STR2b pumice	STR2a pumice	AGN pumice	AMB scoria
VOI (voxels)	314×314×204	200×200×200	200×200×200	300×300×570	268×268×268
Isotropic-voxel length [mm]	0.009	0.009	0.009	0.0067	0.009
Volume [mm^{-3}]	14.66	5.83	5.83	15.43	14.03
Porosity	0.38	0.79	0.84	0.37	0.50
Specific surface area [mm^{-1}]	11.41	26.23	19.66	18.27	20.96
Integral mean curvature [mm^{-2}]	72	−551	−270	432	481
Euler characteristic [mm^{-3}]	−546	−4037	−4356	−68	−651
Fractal dimension	2.60	2.75	2.76	2.68	2.64
Structure thickness [mm]	0.09	0.01	0.01	0.07	0.05
Structure separation [mm]	0.05	0.05	0.08	0.04	0.05
Structure linear density [mm^{-1}]	7.54	14.47	10.83	9.30	10.81
Trabecular pattern factor [mm^{-1}]	−18.88	3.59	−1.24	−61.86	−56.01
N. connected comp./volume [mm^{-3}]	69.63	3.60	9.26	673.79	418.67
Skeleton N. nodes/volume [mm^{-3}]	104.48	778.46	499.49	253.03	547.45
Skeleton N. NODE-to-NODE branches/volume [mm^{-3}]	671.36	5758.23	5157.06	454.14	1945.93
Branches/nodes ratio	6.43	7.40	10.32	1.79	3.55
Isotropy Index	0.83	0.90	0.84	0.60	0.92
Elongation index	0.08	0.03	0.05	0.33	0.05

Zandomeneghi D. et al., Geosphere, 6 (2010) 793-804

Pumice from Campi Flegrei, vesiculated and crystallized

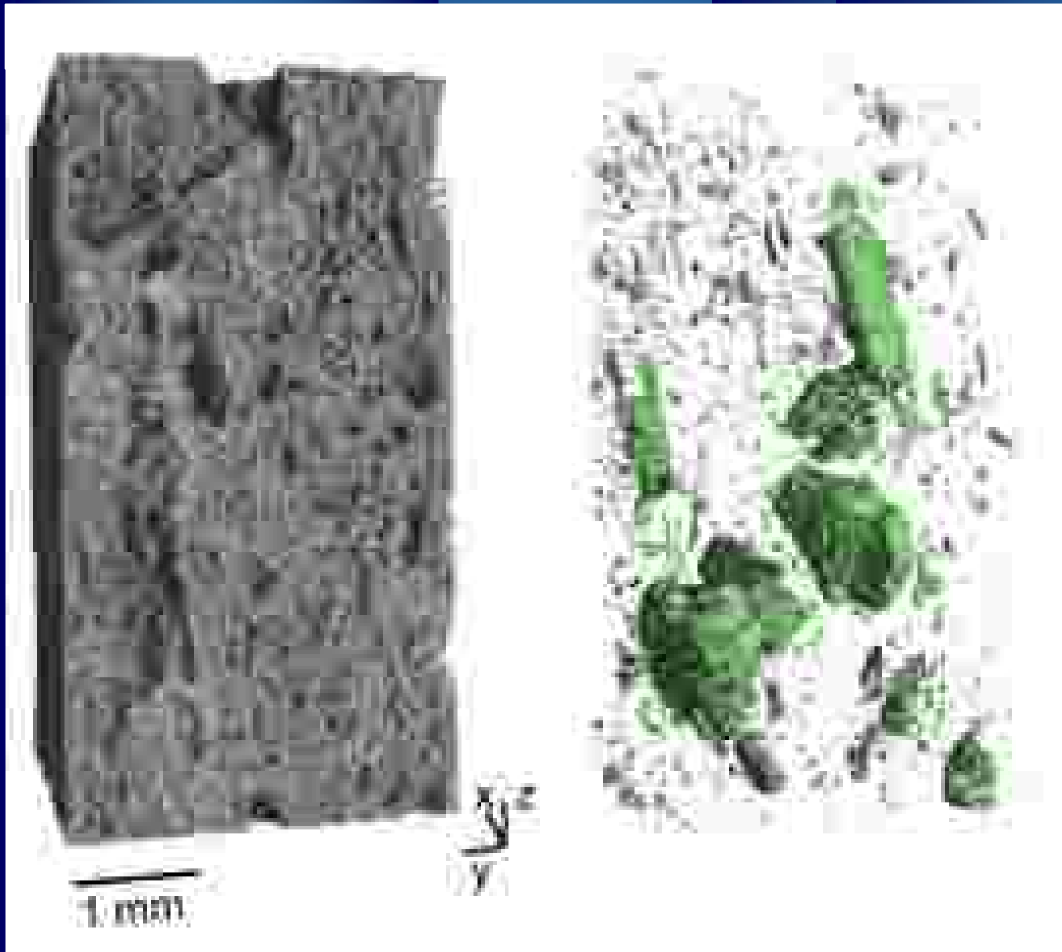

Quite strong *anisotropic distribution* of both vesicles and crystals: *almost axial.*

Vesicles -> 45.0%,
Crystals -> 3.4% (1.2% pyroxenes-2.2% feldspars)

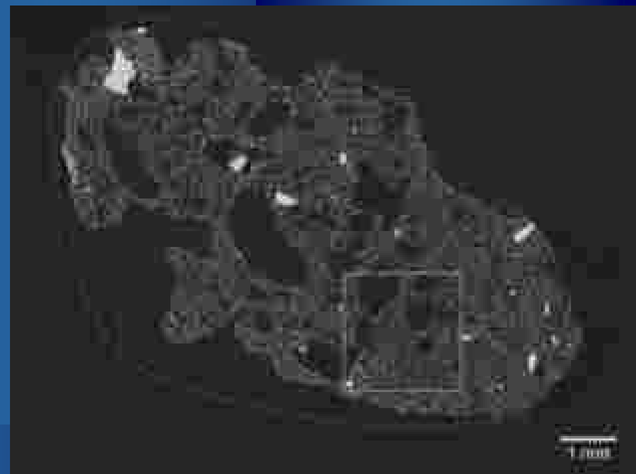

Different methods implemented in *Pore3D* as *Mean Interception Length* and *Shape Preferred Orientation (SPO) analyses.*

Voltolini et al., J. of Volcanology and Geothermal Res., 202 (2011) 83-95

Pole figures for the pumice from Agnano Monte Spina

elettra

We developed a technique based on μCT data to obtain the SPO of both crystals and vesicles, without the requirement of crystalline objects and using a 3D approach

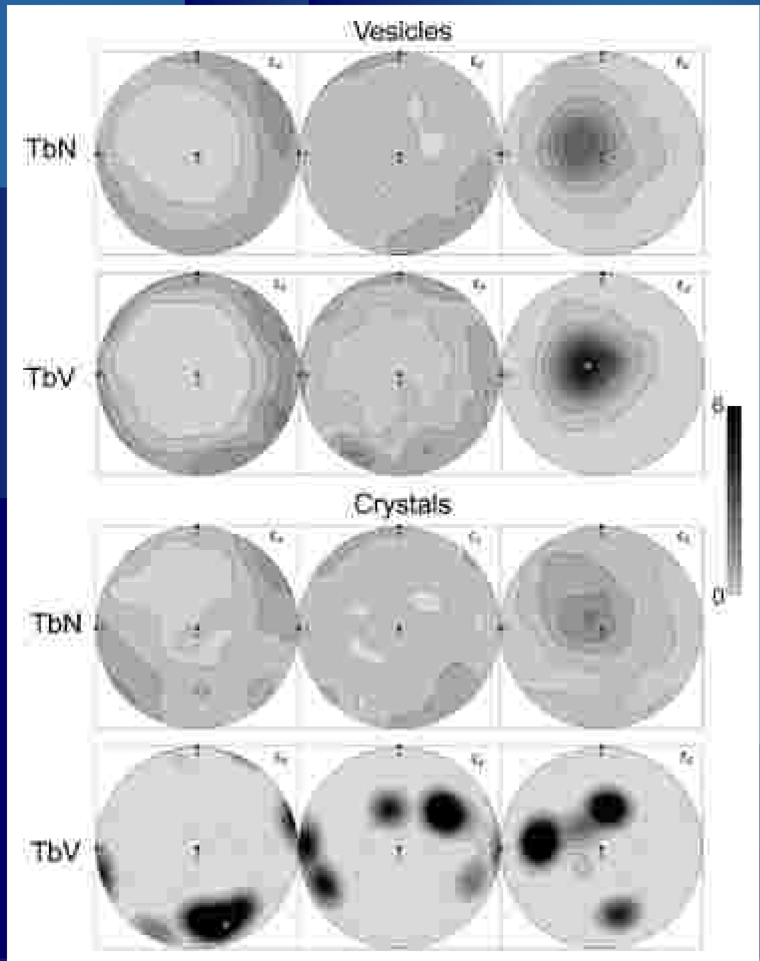

Voltolini M. et al., J. of Volcanology and Geothermal Res., 202 (2011) 83-95 elettra

Conclusions

- Many topics in ***medicine***, ***materials science, cultural heritage***, can be afforded by using 3D quantitative morphological and textural image analysis.

and perspectives

- ***Phase retrieval*** procedures applied to improve phase separation and quantitative analysis.

Acknowledgements

- F. Brun, A. Curri, D. Dreossi, C. Fava, G. Kourousias, E. Larsson, R.H. Menk, S. Mohammadi, R. Pugliese, N. Sodini, G. Tromba, F. Zanini (Elettra)
- F. Arfelli, A. Astolfo, M. Biasotto, E. Castelli, R. Chen, F. Cosmi, R. di Lenarda, R. Longo, M. Maglione, L. Rigon, G. Schena (INFN & Università di Trieste)
- M. Voltolini,(University of Padova (Italy),ESRF)
- F. Bernardini, A. Cicuttin, M.L. Crespo, C. Tuniz, D. Zandomeneghi (ICTP, Trieste)
- M. Polacci (INGV of Pisa, Italy)
- D. Baker, A. La Rue (McGill University, Canada)
- A. Baiano, M.A. del Nobile, P. M. Falcone (Università di Foggia, Italy)
- N. Marinoni, A. Pagani, A. Pavese, P. Vignola (Università di Milano, Italy)
- M. Galiová, M. Holá, J. Kaiser, V. Kanický, K. Novotný (Brno University of Technology, Czech Republic)
- L. Tesei (Istituto Teseo, Trieste)
- G. Bavestrello, D. Pica, S. Puce (Università di Ancona, Italy)

Bibliography

- Principles of Computerized Tomographic Imaging
A.C. Kak & **M. Slaney** , http://www.slaney.org/pct/pct-toc.html

- Pore3D software library: http://ulisse.elettra.trieste.it/uos/pore3d/

- ImageJ software: http://rsbweb.nih.gov/ij/

- DIPlib software: http://www.diplib.org/

-X-ray tomography in material science, **J. Baruchel**, **È. Maire**,
-J.-Y. Buffière, Hermes Science, 2000

- Phase objects in synchrotron radiation hard x-ray imaging,
P. Cloetens *et al* 1996 *J. Phys. D: Appl. Phys.* **29** 133

-Quantitative comparison between two phase contrast techniques:
-diffraction enhanced imaging and phase propagation imaging
E, Pagot *et al* 2005 *Phys. Med. Biol.* **50** 709